Journal of Energy Storage 97 (2024) 112979

Contents lists available at ScienceDirect

Journal of Energy Storage

journal homepage: www.elsevier.com/locate/est

Research Papers

Thermo-economic performance evaluation of thermally integrated Carnot battery(TI-PTES) for freely available heat sources

Syed Safeer Mehdi Shamsi *, Stefano Barberis, Simone Maccarini, Alberto Traverso

[a] Thermochemical Power Group, Dipartimento di Ingegneria Meccanica, Energetica, Gestionale e dei Trasporti, Università degli Studi di Genova, Via Montallegro 1, 16145 Genova, Italy

ARTICLE INFO

Keywords:
Carnot batteries
CO_2
Supercritical CO_2
Pumped thermal electricity storage
Energy storage
Large scale long duration thermal energy storage
Long duration batteries waste heat recovery
Heat source utilization

ABSTRACT

In a scenario driven by non-programmable renewable energy sources (RES) being integrated into the grid, there is a critical need for large-scale energy storage solutions for maintaining grid stability and providing services of frequency regulation as being currently provided by conventional thermal power plants. Among various options, Carnot batteries stand out for their ability to provide GWh scale storage without geographical limitations, at reasonable costs, integrating power to heat to power technologies to thermal energy storage (TES), however at the cost of relatively low Round Trip Efficiencies (RTE). This study delves into a new concept in Carnot battery called Thermally Integrated Pumped Thermal Electricity Storage (TI-PTES) utilizing sCO2 heat pump and power cycles. Thermal integration of heat source in the charging cycle leads to attractive Round Trip Efficiency(RTE) values as compared to conventional PTES. Additionally, using supercritical carbon dioxide (sCO2) as a working fluid offers several advantages of compact designs leading to reduced overall footprint compared to other fluid-based technologies. The study analyzes thermo-economic performance of sCO2 based TI-PTES using an in-house tool WTEMP-EVO; for integration of various industrial and renewable heat sources into the PTES system while exploiting market available thermal energy storage options through a mapping approach.

1. Introduction

Nowadays, governments and energy utilities are promoting ambitious measures to deploy clean and renewable energy resources [1], most of them with stochastic production profiles. As the amount of such variable, renewable generation on the grid increases, grid operators' task of matching generation and demand in real time becomes more challenging, causing energy storage solutions to become the key protagonist at all levels; from decentralized application [2] up to National grid level [3] to a key role player in renewable transition of the global energy system as well as of electric grids all around the world [4]. Nevertheless, the identification and sizing [5] of most suitable energy storage is not always an easy task [6] as this asset has to consider both power production plants' peculiarities, energy off-takers' requests and energy grids stability needs [7]. The electrification of different processes like for example private mobility (via the promotion of EVs [8]) or specific industrial processes and the parallel increase of non-predictable RES power plants, pose the need of identification of different energy storage solutions able to cover the high peaks and deep valleys (during central hours of the days) of the “Duck Curves” [9] that are getting more and more pronounced all around the world [10,11] as renewable energy production continues to grow. For this purpose, bulky energy storages able to flexibly operate like pumped hydro storage(PHS) and to store large amount of energy for a significant number of hours, able to provide large amount of power, rapidly responding to electric market needs as well as grid stability services are necessary. In the end, avoiding if possible to use fossil based power plants which are still required [12] to fill this role of flexibility [13] along with integrated batteries [14] and thermal storage solutions [15]. The present grid conditions are creating an imperative for long duration energy storage (LDES) technologies [16] to ensure supply availability, maximize RES production and replace fossil fueled plants for grid stability.

Energy grids will need two types of LDES [17]: First, that manages daily cycles and provides up to 20 h of storage (solving issues related to “duck curve”), providing grid flexibility services, and another that manages seasonal cycles and provides storage measured in days and weeks. In both cases, this type of bulky energy storage [18] should not be CAPEX intensive, should be location independent and sustainable from a material point of view, competitive than battery storage [19] power-to-hydrogen [20] and pumped hydro storage solutions. Different thermal solutions can therefore be considered for different applications

* Corresponding author at: TPG, Viale Cambiaso, 4, 16145 Genova, GE, Italy.
E-mail address: safeermehdi.shamsi@edu.unige.it (S.S.M. Shamsi).

https://doi.org/10.1016/j.est.2024.112979
Received 15 February 2024; Received in revised form 29 May 2024; Accepted 9 July 2024
Available online 18 July 2024

Nomenclature

CAPEX	Capital Expenditure
CAES	Compressed Air Energy Storage
CC	Charging Cycle
CO2	Carbon Dioxide thermal Cycle
CO_2	Carbon dioxide working fluid
CHP	Combined Heat and Power
COP	Coefficient Of Performance
CSP	Concentrated Solar Power
DC	Discharging Cycle
DHN	Direct Heating Network
EES	Electric Energy Storage
EV	Electric Vehicles
HEX	Heat Exchanger
HP	Heat Pump
HS	Heat Source
KPI	Key Performance Index
LAES	Liquified Air Energy Storage
LDES	Long duration energy storage
LCOE	Levelized cost of electricity
LCOH	Levelized cost of Heat
LCOS	Levelized cost of storage
P2H	Power To Heat
PCM	Phase Change Material
PHES	Pumped Hydro Energy Storage
PTES	Pumped Thermal Energy Storage
RES	Renewable Energy Sources
RTE	Round Trip Efficiency
sCO_2	Supercritical Carbon Dioxide working fluid
sCO2	Supercritical carbon dioxide based cycles
TES	Thermal Energy Storage
TRL	Technology Readiness Level
WHR	Waste heat recovery

Symbols

p_{Out}	Outlet pressure
p_{In}	Inlet pressure
$\Delta p_{\%Loss}$	Pressure loss in heat exchanger
h_{Out}	Outlet enthalpy
h_{In}	Inlet enthalpy
$h_{Out-isoentr}$	Enthalpy at isentropic reference
ε_{HEX}	Effectiveness of the heat exchanger
$\dot{m}_{cold}$	Mass flow of cold side fluid in the heat exchanger
$h_{Out-cold}$	Outlet enthalpy of the cold side fluid exiting the heat exchanger
$h_{In-cold}$	Inlet enthalpy of the cold side fluid entering the heat exchanger
η_{Comp}	Compressor Efficiency
η_{Turb}	Turbine Efficiency
β_{Compr}	Pressure ratio of the compressor
$Q_{HEX-max}$	Maximum total heat transferred in the heat exchanger
Q_{HEX}	Total heat transfer in a heat exchanger
RTE_{el}	Electrical RTE
E_{DC}	Electric energy produced in DC
E_{CC}	Electric energy consumed in CC
P_{DC}	Power produced in DC
P_{CC}	Power consumed in CC
η	Thermal efficiency of DC
$\dot{E}x_{HRU}$	Exergy of the heat source
RTE_{ex}	Exergetic RTE
η_{ex}	Exergetic efficiency of DC
t_{CC}	Charging time(hours)
t_{DC}	Discharging time(hours)

o: power-to-heat [21] and thermal energy storages at different temperatures while promoting coupling with district heating network (DHN) [22] or process industry [23] power-to-heat-to-power, compressed (CAES) [24] and liquid (LAES) air energy storage [25] and Carnot batteries [26].

In this context, Carnot batteries and particularly Pumped Thermal Energy Storage (PTES) systems [27] have progressively gained attention from the scientific and industrial community, being based on a power-to-heat-to-power system integrating a heat pump cycle and a heat-to-power cycle based on rotating machines (volumetric or turbo-machinery), thus being able to offer grid services both during charging and discharging cycles [28]. Different solutions and operating fluids have been studied exploiting well known technologies like ORC [29,30] Brayton [31] and steam cycles [32] as well as innovative energy systems like Stirling [33,34] or sCO2 based cycles. [35]

Among PTES [36] Thermally Integrated PTES (TI-PTES) are attracting more and more interest [37,38] being able to store electric energy with relevant round trip efficiency but also exploiting additional low-mid temperature thermal sources [39] commonly from renewables (like CSP [40,41] biomass or solar thermal) or industrial waste heat recovery (WHR), to boost the charging and/or discharging phases [42].

1.1. Heat source assessment for proposed thermally integrated PTES

WHR is a consolidated approach targeting industrial energy efficiency and decarbonization and it is already recognized as the best practice in many different industrial sectors, particularly to valorize high-temperature waste heat (WH). Nevertheless, as shown in [43] most of the WH come from industrial processes that are qualified as low-grade heat (i.e., <200 °C) which poses several technical challenges for its exploitation towards power production or internal re-use, but that opens the possibility to valorize it via high temperature heat pumps with CO2 (in trans-critical and supercritical status) as a working fluid which is being actively investigated for high-temperature HP applications. At the same time, WH at temperatures higher than 300 °C have already been considered to be valorized via sCO2 power cycles [44,45]. Nevertheless, the possibility to exploit industrial WH with TI-PTES [46] still needs to be fully explored.

In a similar way, high temperature thermal RES (>200 °C) are already exploited to produce renewable power via steam power cycles, ORC and sCO2 [47], The possibility to exploit renewable heat for TI-PTES (even sCO2 ones) has been extensively explored, particularly looking at CSP solar inputs [48,49] lower temperature renewable heat input, like thermal energy coming from solar collectors or from RES driven district heating network [42], integration in ORC based TI-PTES have also been investigated [50]. According to the available literature, it is therefore important to assess more in detail the possibility to integrate in sCO2 based TI-PTES different heat inputs coming from WH (thus also opening opportunities for industrial sectors with low temperature WH) and thermal RES at different temperature levels as shown in Fig. 1.

It is important to note that similar to the WHR, thermal TES which are freely available are being exploited. Meaning the heat sources from CSP plant, collectors or geothermal plants can be utilized to assist the charging of the PTES as a secondary motive i.e. not specifically build for that purpose but assisting when it makes sense economic sense compared to generating power or provide district heating, which is their primary motivation. This can usually happen on the peak shaving hours when the generation in the grid is higher than the requirement and those

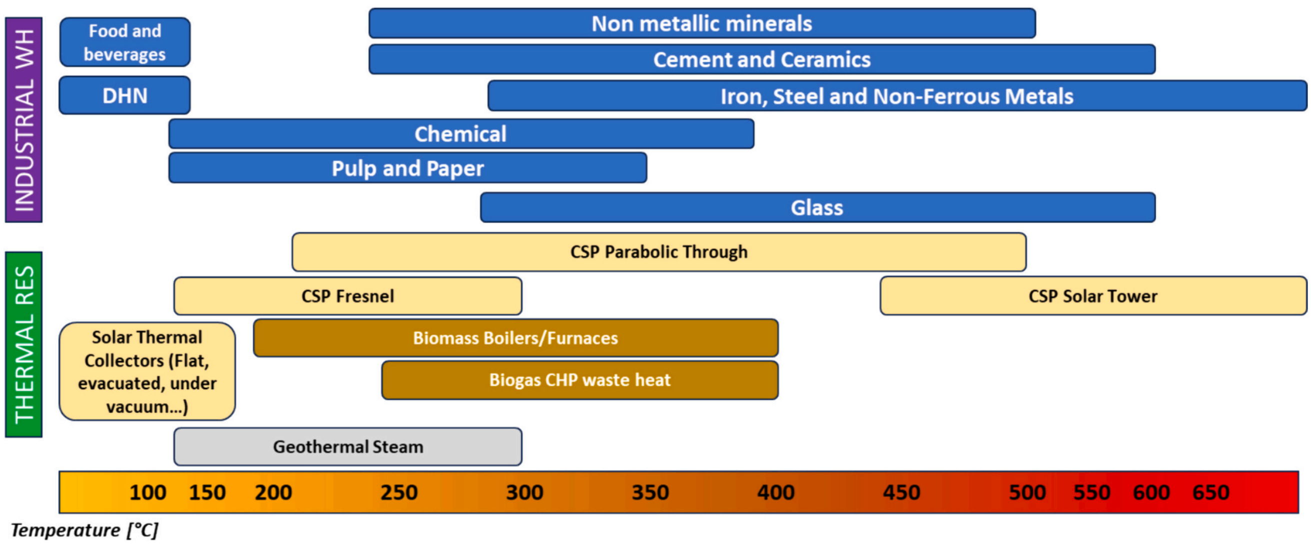

Fig. 1. Heat sources from 100 °C to 650 °C available for valorization by the TI-PTES system.

are the prime times for the PTES to charge where the RES can be utilized.

1.2. Goal and novelty of the study

In this paper, starting from a concept already developed and presented by the authors in previous research studies [43,51], the full potential of sCO2 based TI-PTES is presented, highlighting the relevance of sCO2 heat pump and power cycles towards high RTE valorizing both low and high temperature heat sources and coupling them with commercial TES media at different temperature level. Being inspired by similar research work [52,53], the novelty and ambition of this work is to explore the performance of sCO2 based TI-PTES in different heat source scenarios, mapping the thermo-economic performance and viability of the proposed PTES exploiting different freely available heat sources (e.g. industrial Waste heat recovery (WHR) or thermal RES) at various temperature levels, thus aiming to minimize the environmental impact of the TI-PTES targeting enhanced performances from an energetic, exergetic (maximizing RTE) and economic point of view.

In order to evaluate the suitable storage for a given heat source (HS) temperature from a thermo-economic point of view in light of the available TES materials on the market shown in Fig 2. A range of storage temperature and market available materials are selected and plotted for performance against the available heat source temperatures generating a correspondence map for a selected range of storage and available heat sources. Providing insights for market available storages at different temperatures suitable for various industrially available heat sources thus inspiring the development and deeper investigation of RES heat/WH-driven sCO2 PTES case studies.

2. System description

For evaluation of different heat sources at different temperatures and different TES temperatures/material, the idea is to use configurations that are efficient as well as practically viable. Despite sCO2 TI-PTES not being extensively studied so far [35] it is clear that there might be some complex configurations of both the charging and discharging cycles which may seem to eventually be more thermo-economically competent [54] however, simpler configurations (simple or recuperated cycles) have been employed in many of the ongoing and past sCO2 projects [47] and studies [55] as they have more operational stability in addition to the reduced capital and operational cost.

The TI-PTES configurations used in this study are shown in Fig. 3. Two type of charging cycles are used: Simple charging cycle consists of four basic components required to complete the cycle while the recuperated charging cycle have an additional component; the recuperator. The two TI-PTES configurations are then:

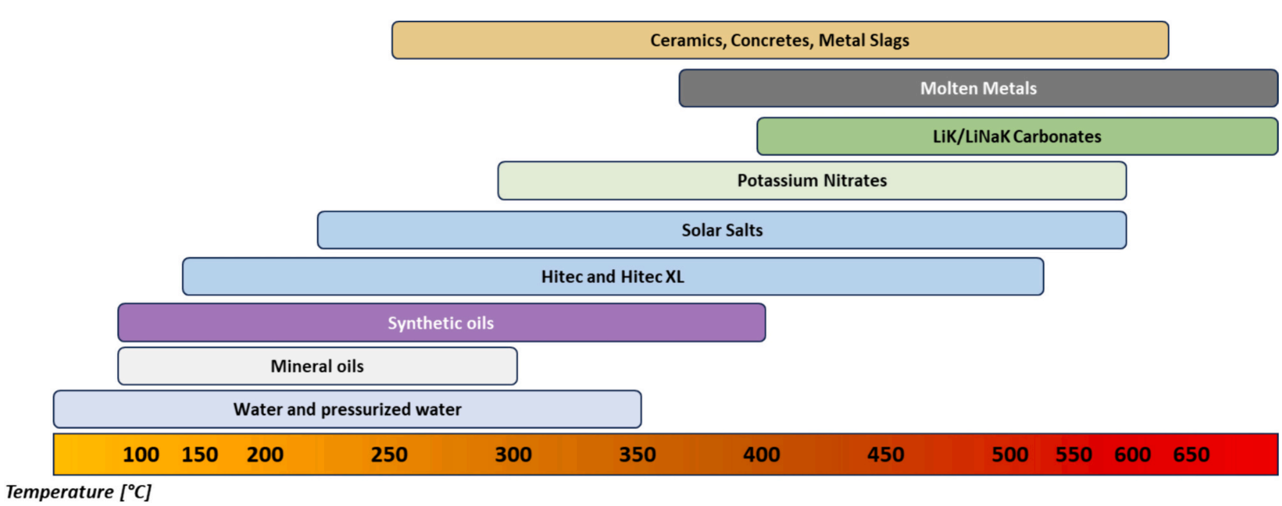

Fig. 2. Commercially available thermal storages at temperature ranges from 100 °C to 650°.

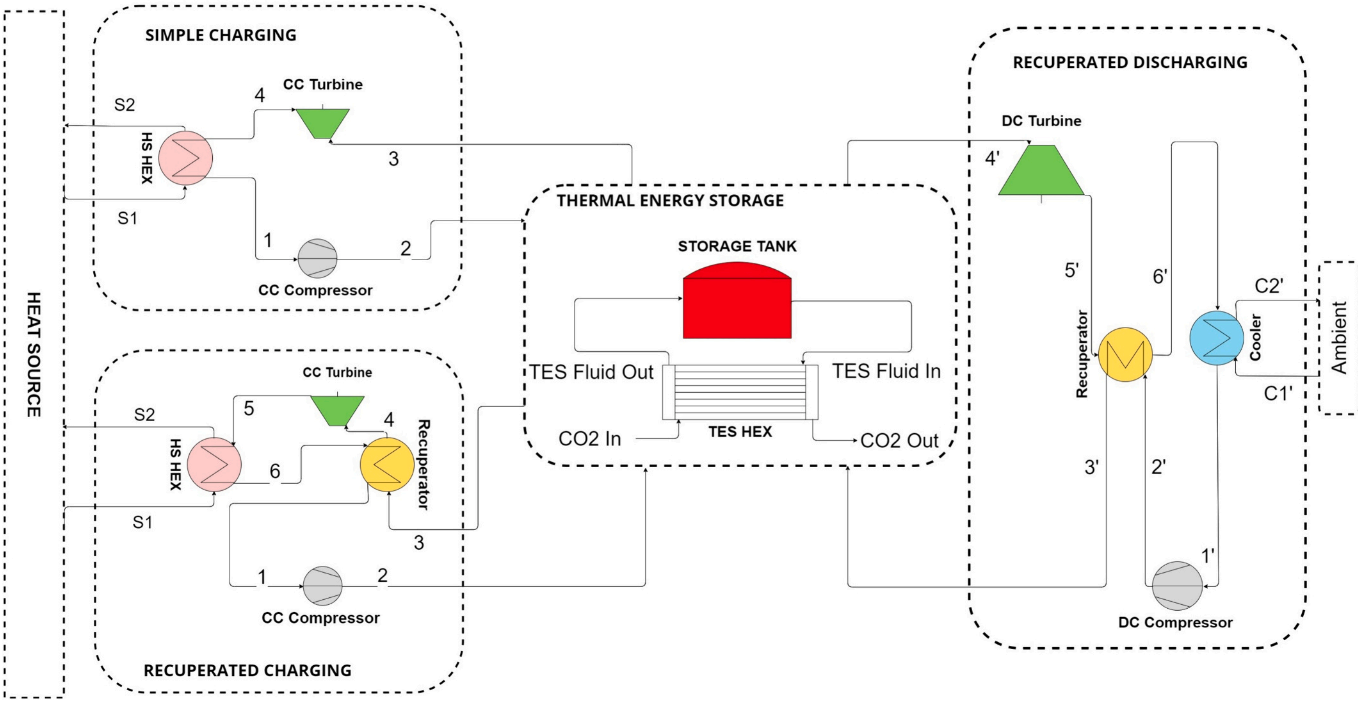

Fig. 3. TI-PTES configurations: simple charging recuperated discharging, recuperated charging recuperated discharging.

(a) Simple charging coupled to a recuperated discharging cycle through TES
(b) A recuperated charging cycle coupled to a recuperated discharging cycle through TES.

Starting from the simple charging cycle, the working fluid's (which in this case is sCO2) starting point is the compressor inlet (1), it passes through the compressor, where the pressure as well as enthalpy of the working fluid is increased, (2) fluid then goes to the TES HEX where TES fluid enters at one end and sCO2 enters the other. sCO2 being the hot fluid, transfers its heat to the TES fluid and exit at a lower temperature (3) enters a cold turbine, after expansion (4) sCO2 enters the heat source HEX where the sCO2 takes the heat from the given source and repeats the cycle. In the recuperated charging cycle, the recuperator is installed after the TES, the sCO2 enters the recuperator (3) and exits at turbine inlet(4) transferring the heat to the sCO2 after the HS HEX (6) and compressor inlet (1) while the rest of the cycle points are similar to the simple charging.

The Thermal energy storages system (TES) is modelled with two entities: Storage material container and a heat exchanger i.e. TES HEX, that transfers heat to or from the thermal energy storage material depending whether the system is operating in charging mode or discharging mode respectively. The thermal nature of the TES considered for this study is sensible(temperature changes as the heat is added) to better match with the sCO2 profile. TES fluid is the reference to the medium with which the thermal storage exchanges heat with sCO2 in TES HEX. If the storage material is liquid then the material itself can flow in TES HEX, however if the storage is a solid material, another entity can act as a TES fluid to transfer heat between the TES HEX and the storage material itself. TES fluid and sCO2 will pass through same passages regardless of the process but in opposite directions for charging and discharging. There are high temperature and pressure valves available in the market [56] for sCO2 also being used in previous studies and HEX designs [57,58]; which can facilitate such operation.

The recuperated discharge cycle starts at (1′) cold compressor whose inlet conditions are nearly ambient and near to the critical point to assist in power saving for compressor operation. (2′) After compressor, sCO2 passes through the recuperator gets preheated and (3′) enters the TES HEX extracts the heat from the TES HEX attaining the peak temperature and then (4′) goes through the hot expander, after which it (5′) passes through the recuperator and gives off any extra heat (6′) finally passing through the cooler to come back to the compressor inlet conditions again. Other than the TES, all the components of the charging and discharging cycle are separate.

Table 1 presents the list of assumptions used in the computation of all the cycles in TI-PTES operation (charging and discharging), and the list of variables. Since the TES HEX is shared, the high pressure side of both the CC and DC are fixed at suitable value of 250 bar where the commercially available heat exchangers can be exploited. To reach the maximum TES temperature for any configuration, CC relies on the pressure ratio. Therefore, fixing the upper side pressure makes much more sense than fixing the lower side pressure for the CC, as not to obtain pressure values on the high pressure side, unsuitable for market available heat exchangers. In case of DC, high pressure side as well as the

Table 1
Constraints for thermodynamic modelling.

Parameter	Value	UoM
Machine Constraints:		
Compressor isentropic efficiency	80	%
Turbine isentropic efficiency	80	%
HEX pressure losses	1	%
ΔT Pinch	10	K
DC Recuperator Effectiveness	80	%
Electrical and Mechanical Eff.	99	%
Environmental Constraints:		
Temp. reference state (exergy)	15	°C
Pressure reference state (exergy)	1	bar
Ambient temperature	25	°C
Cycle Constraints:		
Charging:		
CC high pressure	250	bar
Discharging:		
DC high pressure	250	bar
DC low pressure	85	bar
Coolant inlet temperature (Air)	25	°C
Coolant exit temperature (Air)	45	°C

low pressure side is fixed. The DC lower pressure at the inlet of the compressor has been kept at 85 bar as was found appropriate according to authors' previous study [43].

As CC and DC are independent in terms of operation and turbomachinery components, being only integrated with the thermal storage, two benefits can be highlighted: i) the CC turbine can expand far from the critical point as well as the bell curve, having higher produced work values; ii) As the lower pressure side of the CC and DC are independent, it is possible to increase the expansion ratio of the discharging turbine, increasing the overall performance of the system.

This study will use the energy storage temperatures ranging from 400°C to 650 °C(with 50 °C interval). The thermal storage material used for this purpose and their constraints are reported in Table 2. The range of storage temperatures selected is similar to previous studies [43,51]. The purpose of selection of those temperature ranges are can be attributed to utilization of readily market available storage materials that are employed in other matured application such as CSP. Also the performance of sCO2 cycles are particularly better around these temperature ranges than other fluids, So to harness the higher efficiencies of sCO2 cycles as well as exploitation of market available TES materials, this range of storage temperatures is the most optimum.

For the case of molten salts and thermal oils, the storage container can be considered as two tank configurations where the storage medium is the heat transfer fluid itself, exchanging heat passing through the TES HEX. In most configurations of Packed bed storage, there are no two separate tanks but rather a single unit, however, there is a thermocline in that case within the unit with a high temperature point and a low temperature point which serve the same purpose.

For solid packed bed, usually air, molten salts or thermal oils are used as the heat transfer fluid. The use of liquid TES fluid could guarantee a constant discharge temperature. But to provide constant outlet temperature using solid bed and Air, it will need to be oversized considerably or alternatively one can let the outlet temperature drop at the expense of reducing thermal efficiency. For our study, liquid options cannot be utilized owing to the operating temperature of the packed bed storage. So air is utilized as the TES fluid and a constant discharge temperature is assumed following the necessary sizing (where the packed bed is sized based on Air volume flowrate needed to guarantee a proper heat exchange) and cost to ensure the constant temperature during the process using an approach already proposed in [59] which also highlights the consequences of dropping temperatures.

The thermal energy storage is coupled with the HS temperature from 150 °C to 600 °C (with 50 °C interval) in the charging cycle, encompasses low grade, medium and very high heat sources as reported in Table 3. The heat from all the sources in these temperature ranges is present in the form of Air, steam or exhaust gases with different compositions. The HS HEX acts as a heat recovery unit for the TI-PTES. Different type of sources are available at similar temperature ranges, however with different carrier mediums. To make things more comparable, the medium of the heat sources is considered to be air for all the heat source temperatures(as it is the more dominant of the mediums in which the heat sources are available. Although with similar fluid properties on both sides for HS HEX the cost comparison for different HS becomes more meaningful. The difference in temperatures of available heat sources is however, not negligible. The sizing and cost of the HS HEX (heat recovery unit) are accounted for in terms of the material changes that should be done for recovering low-mid temperature (150 °C–400°C) and high temperature(400°C–600 °C) heat sources.

Table 3
Properties and constraints of heat source.

Heat source medium	Air	
Temperature range variation	150–600	°C
Interval for mapping	50	°C

Each thermal storage temperature generated by 50 °C interval in the given range of thermal storage temperature variation is coupled with each HS temperature generated in the given HS range to produce 45 unique combinations which were then analyzed for the two TI-PTES configurations.

3. Materials and methods

All the thermodynamic computations were done using a modified version of WTEMP-EVO, a component-based in-house thermo-economic simulation tool. It is developed in MATLAB®, integrating Coolprop [63] libraries for fluid properties, and it can simulate energy systems through the assembly of the desired layout, as explained in [64]. The tool whose workflow is presented in Fig. 4, implement the component-level characteristic equations for mass and energy balances, and pressure computation; some of them are reported in Appendix D.

Since the TI PTES systems basically consists of two separate cycles, with separate components for charging and discharging, the simulation separates the computation of the two cycles, indirectly connected by imposing the equivalence of the temperatures of the TES, and the amount of energy and mass stored in it. In practice, the code firstly computes the DC, and then uses the results to initialize the computation of the CC. To be more precise, since the discharging layout consists of a recuperated cycle regardless of the charging cycle being used, the minimum TES temperature for both charging and discharging, depends on the inlet temperature of the TES fluid in TES HEX in the DC which is dependent on the effectiveness of the recuperator. For this reason the DC is computed first, and then the low temperature tank (TES fluid inlet temperature in the TES HEX in the DC) is used to set the boundary conditions in the CC.

After the solution of the cycle some of the main thermodynamic performance parameters analyzed are reported as follows:

$$COP = \frac{\dot{Q}_{TES\_CC}}{P_{CC}} \tag{1}$$

$$\eta = \frac{P_{DC}}{\dot{Q}_{TES\_DC}} \tag{2}$$

$$RTE_{el} = \frac{E_{DC}}{E_{CC}} = \frac{P_{DC} \cdot t_{DC}}{P_{CC} \cdot t_{CC}} = COP \cdot \eta \tag{3}$$

The electrical round trip efficiency can be seen in eq. 3 which is the ratio of electrical energy generated by the discharging cycle to the

Table 2
Properties and constraints of thermal energy storage materials.

Storage	Density (kg/m^3)	Specific Heat (kJ/kg K)	Thermal conductivity (W/m K)	Heat transfer fluid	Design Storage temp. (°C)	Maximum Allowable Storage temp. (°C)	Minimum allowable storage temp (°C)
Silicon oil FRAGOLTHERM-X-75-A [60]	548	2.26	0.064	Oil	400	400	−40
YARA MOST [61]	1913	1.43	0.52	Salt	450	450	220
HITEC XL [62]	1877	1.42	0.52	Salt	500	500	220
Solar Salt [62]	1740	1.53	0.5	Salt	550	550	250
Packed bed [59]	2850	1.17	1.5	Air	600 & 650	800	25

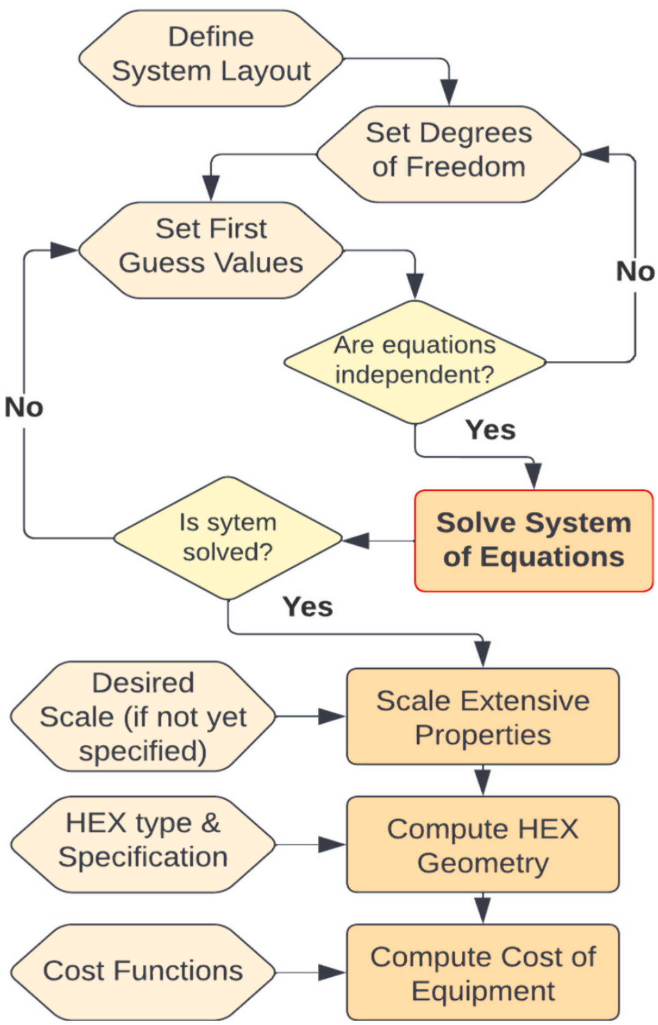

Fig. 4. Work flow of the WTEMP-EVO tool.

electrical energy consumed in the charging cycle. The electrical energy in the charging or discharging can be further divided into power consumed or generated, multiplied by the time for charging or discharging. So if the power in CC and DC of the TI-PTES is kept equal to provide equal grid flexibility, the RTE will be accounted for by the time taken for charging and discharging. It is possible to identify a formulation of RTE which only depends on the thermodynamics of the cycles, considering the hypothesis of no losses within the thermal energy storage(i.e. $Q_{TES\_CC} = Q_{TES\_DC}$); this argument, even though strong considering the amount of storage time in some cases; is useful from a comparison and design point of view so that the total energy that is charged into the TES, is fully discharged as well. According to such hypothesis and starting from the definition of RTE based on energy, a formulation implementing the thermal power value exchanged with the TES and the CC and DC times can be identified, which leads to an expression showing COP and power cycle efficiency (η).

Similarly, in order to take into account the contribution of the HS used in the recovery unit(HS HEX), an exergetic RTE has been evaluated for each solution to establish a fair comparison between the different cases, on a thermodynamic point of view. The following formulae in eq. 4 and 5 illustrate the exergy utilization in the two cases. The exergy has been computed using a reference state of 1 bar and 15 °C, and considering only the exergy exchange within the system (for instance, only the exergy exchanged within the HS HEX, and not the whole exergy available in the WH).

$$RTE_{ex} = \frac{P_{DC} \cdot t_{DC}}{\left(P_{cc} + \dot{E}x_{HRU}\right) \cdot t_{CC}} = \quad (4)$$
$$= \frac{\eta}{-\frac{1}{COP} + \frac{\dot{E}x_{HRU}}{\dot{Q}_{CC\_TES}}} = RTE_{el} \cdot \frac{1}{1 + \frac{\dot{E}x_{WHRU}}{P_{cc}}}$$

$$\eta_{ex} = \frac{P_{DC}}{\dot{E}x_{WHRU}} \quad (5)$$

The total cost of the PTES is calculated using the cost functions given in Appendix B. The components and the references are also listed with the cost function themselves. With so many configurations observing variety of temperatures and pressures, cost functions in the literature do not encompass the thermodynamic parameters obtained for all combinations of TES and HS. Therefore, alternative cost functions are used where necessary. However, if the cost value trends become much abrupt using two different cost functions, the one that is more influential in the given domain of operation is used for calculating the cost instead. Some other KPIs discussed are as follows:

$$mCO2\ ratio\ in\ Hot\ HEX\ per\frac{kg}{s}of\ TES\ flow = \frac{mCO2\ in\ CC}{mCO2\ in\ DC} \quad (6)$$

$$ratio\ of\ TES\ fluid\ mass\ flow\ rate = \frac{Massflow\ TES(DC)}{Massflow\ TES(CC)} \quad (7)$$

$$Q_{TES\ total} = Q_{TES} \times t_{CC\ or\ DC} \quad (8)$$

$$Specific\ Cost\ of\ Storage\left(\frac{\$}{Wh}\right) = \frac{Cost\ of\ Charging\ Equipment}{Q_{CC\_TES} \times t_{CC}} \quad (9)$$

$$Specific\ Cost\ of\ Generation\left(\frac{\$}{Wh}\right) = \frac{Cost\ of\ Discharging\ Equipment}{P_{DC} \times t_{DC}} \quad (10)$$

4. Results and discussion

The information flow of the results is as follows: The 45 unique combinations of TES and HS temperatures are first analyzed for TI-PTES configuration of simple charging cycle after assessing the necessary thermodynamic KPIs; TES and HS combinations are then subjected to the TI-PTES configuration that uses recuperated charging cycle. From both the TI-PTES configuration, the higher performing configuration for each TES and HS combinations is selected and then subjected to further thermo-economic analysis.

4.1. Thermodynamic assessment

For the thermodynamic evaluation of the different HSs coupled with different TES temperatures, the results are discussed in the same arrangement, the models were generated. Discussing the discharging cycle first, that is optimized for maximum possible efficiency while providing necessary boundary conditions of the TES lower temperature value, TES characteristics are described following the discharging while the charging cycle which is influenced by both the TES as well as the freely available HS parameters, is discussed in the end. It is important to note that throughout this sequence of information transfer, the thermodynamic calculations have been carried out for constant TES characteristics i.e. (1)The inlet and outlet of the TES temperature remains the same in the charging and discharging cycle regardless of the HS (2) the mass flows of all the fluids in the TI-PTES system are reported per 1 kg/s of mass flow rate of the TES in both the charging and discharging cycle for thermodynamic calculations, which are then scaled up for the actual plant size in MW for which the efficiencies of turbomachinery are assumed.

4.1.1. Discharging cycle

The freely available HS being used in the charging cycle has no effect on the discharging cycle as DC is coupled to CC only through the TES.

There are six TES temperatures(400°C, 450 °C, 500 °C,550°C, 600 °C,650 °C) for which DCs are modelled and optimized for highest efficiency. The thermodynamic properties and points are listed in Table 4 for discharging cycles integrated with TES at certain temperatures. As the upper storage temperature, set by the user for each configuration and the mass flow rates are per kg/s of TES fluid, the rest of the thermodynamic points as well as the mass flow rate of CO2 and cooling fluid which in this case is ambient air, are calculated using the other boundary constraints. The pressure ratio, compressor inlet conditions as well as the cooling fluid's inlet and outlet condition remain the same for all six models, other than the machine constraints already in place. The amount of total heat transfer in the HEX of DC and the power generated by the turbomachinery for 1 kg/s of mass flow rate of TES in DC is shown in Table 5. The net power output in the discharging cycle is arbitrary with the increasing storage temperatures rather than showing an increasing trend. Strong dependance on the storage material characteristics i.e. specific heat capacity is the reason for such trends, Specific heat capacity being different for each of the TES material used for the appropriate storage temperature have the effect on mass flow rates, hence the power outputs. The efficiency however follow an increasing trend with increasing storage temperatures as it is independent of the extensive parameters of the cycle.

Table 4
DC thermodynamic points and CO2 mass flow (per 1 kg of TES mass flow) for TES temperatures variation from 400 °C to 650 °C.

	p(bar)	t(°C)	h(kJ/kg)	s(kJ/kgK)	m(kg/s)
400 °C					
1'	85.00	35.00	308.84	1.35	1.66
2'	250.00	70.70	340.39	1.37	1.66
3'	245.00	183.72	555.81	1.93	1.66
4'	240.10	389.85	831.84	2.43	1.66
5'	88.50	293.67	739.24	2.47	1.66
6'	86.73	105.56	523.82	2.00	1.66
C1'	1.50	25.00	424.39	3.83	17.73
C2'	1.48	44.85	444.39	3.90	17.73
450 °C					
1'	85.00	35.00	308.84	1.35	1.11
2'	250.00	70.70	338.67	1.37	1.11
3'	245.00	212.90	602.84	2.02	1.11
4'	240.10	439.85	895.19	2.52	1.11
5'	88.50	340.49	797.24	2.56	1.11
6'	86.73	113.59	533.07	2.03	1.11
C1'	1.50	25.00	424.39	3.83	12.45
C2'	1.48	44.85	444.39	3.90	12.45
500 °C					
1'	85.00	35.00	308.84	1.35	1.13
2'	250.00	70.70	338.67	1.37	1.13
3'	245.00	244.09	645.93	2.11	1.13
4'	240.10	489.85	957.36	2.61	1.13
5'	88.50	387.13	851.10	2.65	1.13
6'	86.73	121.91	543.85	2.06	1.13
C1'	1.50	25.00	424.39	3.83	13.23
C2'	1.48	44.85	444.39	3.90	13.23
550 °C					
1'	85.00	35.00	308.84	1.35	1.20
2'	250.00	70.70	338.67	1.37	1.20
3'	245.00	276.88	689.34	2.19	1.20
4'	240.10	539.85	1019.73	2.69	1.20
5'	88.50	433.61	905.36	2.73	1.20
6'	86.73	130.50	554.70	2.08	1.20
C1'	1.50	25.00	424.39	3.83	14.78
C2'	1.48	44.85	444.39	3.90	14.78
600 °C					
1'	85.00	35.00	308.84	1.35	1.04
2'	250.00	70.70	338.67	1.37	1.04
3'	245.00	310.88	733.11	2.27	1.04
4'	240.10	589.85	1082.43	2.76	1.04
5'	88.50	479.97	960.08	2.80	1.04
6'	86.73	139.34	565.64	2.11	1.04
C1'	1.50	25.00	424.39	3.83	13.34
C2'	1.48	44.85	444.39	3.90	13.34
650 °C					
1'	85.00	35.000	308.835	1.350	1.038
2'	250.00	70.701	338.673	1.368	1.038
3'	245.00	345.789	777.282	2.342	1.038
4'	240.10	639.850	1145.494	2.832	1.038
5'	88.50	526.211	1015.293	2.874	1.038
6'	86.73	148.413	576.684	2.136	1.038
C1'	1.50	25.000	424.393	3.832	13.909
C2'	1.48	44.850	444.387	3.903	13.909

4.1.2. *Thermal energy storage*

The working fluid or heat transfer fluid as shown in Table 6, is a molten salt or thermal oil itself or air in case of the configurations that use packed bed as a thermal storage material. The upper limit of storage temperatures are constrained by boundary condition whereas the lower limit of storage temperature are set by the discharging cycle and can be seen in Table 6. The TES material along with the TES HEX makes up the thermal energy storage. As mass flow rate of TES has been considered equal in CC and DC for thermodynamic assessment, the ratio between the mass flow rate of sCO2 of CC to DC per 1 kg of TES fluid mass flow can be seen in Table 6. The mass flow rate of CO2 in the CC is calculated by the TES temperatures, TES mass flow rate and approaching temperature constraints. So the mCO2 in the TES HEX during charging remains the same for a given TES temperature, the mass flow rate of HS is set by the mCO2 in CC. So with changing temperatures of HS, the mass flow rate of the HS will also change whereas the mass flow rate of CO2 in CC will only change if the TES changes.

Besides, the mass flow rate in discharging cycle that is dependent upon the highest efficiency achievable, the heat transfer during discharge is quite simple as the TES is the hot fluid and CO2 is the cold fluid whereas the mCO2 during charging being the hot fluid have additional complexities and the mass flow rate of CO2 in CC is influenced by an additional factor of internal pinch point, which determines the outlet temperature of the CO2 from TES HEX as well as the mass flow rate of CO2 in CC for a fixed temperatures and mass flow rate of given TES which is also depicted in Appendix C.

4.1.3. *Charging cycle*

After the modelling of discharge cycle, and using it to define useful parameters for the TES, the charging cycle has been evaluated for different HSs coupled with different TES temperatures providing a correspondence map between the two, for different TI-PTES parameters that can help a designer to identify the best coupling based on their interest and application. The maps have been generated for the storage temperatures of 400 °C to 650 °C with the HS couplings of 150 °C to 600 °C with intervals at 50 °C with total of 45 configurations each evaluated with a unique TES and HS coupling to generate a unique PTES. Some configurations of TI-PTES with as low as 50 °C gap between the TES and HS temperatures may seem impractical for utilization, nevertheless they provide important information for the general trend that is followed by the key parameters and help in understanding the best coupling behaviors. The thermodynamic properties along with the operating points are listed in detail for the charging cycle in the additional documentation provided with this article.

Fig. 5(a) shows the pressure ratio (β) mapping of the charging cycle for the various coupling of TES and HS. Considering it being a simple CC, the compensation of temperature gap between HS and TES is directly dependent on the pressure ratio i.e. higher the temperature difference between the HS and TES higher is the pressure ratio of the CC and vice versa. Beyond the temperature difference itself, β seems to be slightly affected by the actual temperature values of HS and TES as well, for example a TI-PTES with TES temperature 400 °C and HS 350 °C and

Table 5
DC power (per 1 kg/s TES mass flow) for TES temperatures variation.

Storage temp (°C)	Compressor (kW)	Hot HEX (kW)	Recuperator (kW)	Turbine (kW)	Cold HEX (kW)	Net power (kW)	Efficiency (%)
400	51.50	455.04	355.13	151.12	355.13	99.62	21.89 %
450	32.79	324.54	293.25	107.65	293.25	74.86	23.07 %
500	33.25	350.54	345.85	118.40	345.85	85.15	24.29 %
550	35.50	397.08	421.44	136.08	137.45	100.58	25.33 %
600	30.67	362.66	362.66	125.75	409.51	95.08	26.22 %
650	30.67	382.28	455.36	133.82	455.36	103.16	26.98 %

Table 6
Thermodynamic characteristics of TES per 1 kg of TES mass flow.

Maximum storage temperature (°C)	Minimum storage temperature (°C)	mCO2 ratio in TES HEX
400	193	0.718
450	223	1.091
500	254	1.085
550	286	1.021
600	320	1.183
650	355	1.177

another TI-PTES with TES temperature 650 °C and HS 600 °C have same temperature difference of 50 between HS and TES, have different β requirements of 1.48 and 1.36 respectively, this behavior can be attributed to the state of the working fluid itself which has different fluid properties especially specific heat capacity at different temperatures.

Co-efficient of performance (COP) follows the trend similar to that of the pressure ratio, as can be seen in Fig. 5(b). For the charging cycle, heat delivered to the TES storage has been decided by the DC, so it remains constant for the change in the HS coupling. For a particular TES temperature, the coupling HS temperature does not have any effect on the amount of heat that will be stored in the TES. The net work done on the charging cycle however, is affected by the HS temperature. Lower the HS temperature, higher is the amount of work required by the heat pump charging to deliver the specific amount of heat required for the particular TES temperature. For a simple configuration of a charging cycle such as this, the required work is compensated by the change in the pressure ratio. For a lower temperature HS, the pressure ratio, consequently the work done is larger. Therefore, for a given TES temperature as everything else remains the same, COP has the same trend as β of CC.

4.1.4. Performance assessment and benchmarking

Based on the thermodynamic model of simple charging, discharging developed to study the various TES and HS temperature couplings; electric round trip efficiency and exergetic round trip efficiency have been calculated as can be seen in Fig. 6, quantifying the performance of the each combination of TES and HS for each PTES.

The discharging cycle thermal efficiency is only affected by the TES temperature as they are independent from the HS, looking at the horizontal RTE trends in Fig. 6(a), it is only influenced by the COP of the CC whereas the vertical trends are influenced by the COP of CC as well as the DC thermal efficiency. With the change of TES temperature both the COP as well as the discharge cycle efficiency change. Nevertheless, the trends of RTE seem similar to that of the COP, because COP has more influence on the RTE than the discharging efficiency. The similar color pattern in the diagonal shows a strong influence of the temperature gap between the storage and HS temperature on the RTE of the TI PTES. For 50 °C temperature gap between the storage and HS temperature, all the RTEs are above 100 %, meaning that the amount of electrical charging power required to store the heat to a certain TES is smaller than the amount of electricity produced in the discharging cycle thanks to freely available HS TI-PTES is coupled with in CC. But as the temperature gap between the TES temperature and the HS becomes larger, the effect of the HS starts to reduce with the lowest RTE being 31.69 % for the largest gap of 500 °C for the TI-PTES configuration with 650 °C storage temperature and 150 °C HS temperature. Depending upon the cost of electricity, it can definitely make sense to have a lower temperature HS coupled with high temperature storage if the prices are mostly negative, to get a higher use of heat pump cycle even if it has a lower RTE. But usually the combinations with above 50 % RTE can be acceptable for any market.

Although freely available heat is being used in charging cycle hence supporting the heat pump cycle by elevating the temperature to somewhat desirable point to pump heat into TES minimizing the losses of turbomacinery. The actual measure of the energy input in the charging cycle and the energy retrieved during the discharging cycle however, is through the exergetic RTE shown in Fig. 6(b). It considers the energy contributions of both the HS and the heat pump cycle. For all the configurations, the exergetic RTE is below 50 % which means that for the work that is put into the charging cycle by collective efforts of the freely available HS and the heat pump, less than half of it is retrieved in the discharging cycle. The exergetic loss seems to increase for the larger gap between the source temperature and the storage temperature. The fulfillment of the temperature gap as dependent on the heat pump cycle is directly related to increase in the amount of work to be done by the turbomachines to store the heat up to the required temperature in the charging cycle, which are subjected to isentropic loss. Larger the gap, greater is the work done by the turbomachines, consequently higher losses by irreversible behavior of turbomachines; that is why if there is no HS present, the electrical RTE will be lower than the exergetic RTE for that given temperature of storage because having HS, decreases the irreversible losses of the turbomachinery during the charging cycle. The values of exergetic RTE for our selected temperatures of storages and HSs are between 30 % to 50 %, a smaller magnitude compared to the electrical RTE. Similar to electrical RTE, smaller temperature gaps between TES and HS temperatures, as well as higher absolute temperatures of TES and HS are favorable as compared to the lower TES temperatures as they decrease the efficiency in the DC.

4.1.5. Recuperated charging cycle

It is evident from the TI-PTES pressure ratio maps of simple charging cycles, that the pressure ratios for some combinations of TES and HS are too impractical for realization even with series of compressors and turbines. In simple charging cycle, the compressor inlet temperature is constrained by the HS temperature i.e. the compressor inlet is 10 K below the HS temperature. One way to decrease the pressure ratio is to increase the inlet temperature of the compressor by releasing it from the constraints of the HS, which can be done by the addition of a recuperator. The heat is recuperated from the high pressure side stream to the low pressure side stream making the inlet temperature of the compressor 10 K below the TES HEX sCO2 stream outlet temperature in the charging cycle. It is important to note that the recuperator elevates the temperature of sCO2 on the low pressure side after sCO2 has already taken heat from the HS HEX. Therefore, the cases in which the HS temperature is higher than the sCO2 TES HEX outlet temperature, the recuperator cannot be used, restricting the recuperator use to particular cases as shown in Fig. 7. Coincidently, the configurations in which the recuperators can be used are the ones which actually need benefitting from it for decreasing the pressure ratios.

Pressure ratio CC

Thermal energy storage (°C) \ Heat Source(°C)	150	200	250	300	350	400	450	500	550	600	650
650	37.63	22.94	14.58	9.60	6.53	4.56	3.27	2.39	1.79	1.36	NaN
600	27.75	17.00	10.86	7.19	4.92	3.46	2.49	1.83	1.38	NaN	NaN
550	20.26	12.48	8.02	5.35	3.68	2.60	1.89	1.40	NaN	NaN	NaN
500	14.63	9.07	5.87	3.94	2.73	1.94	1.42	NaN	NaN	NaN	NaN
450	10.45	6.54	4.26	2.88	2.01	1.44	NaN	NaN	NaN	NaN	NaN
400	7.45	4.70	3.09	2.11	1.48	NaN	NaN	NaN	NaN	NaN	NaN

(a)

COP

Thermal energy storage (°C) \ Heat Source(°C)	150	200	250	300	350	400	450	500	550	600	650
650	1.16	1.26	1.39	1.55	1.77	2.07	2.50	3.23	4.61	8.30	NaN
600	1.22	1.34	1.49	1.70	1.99	2.41	3.10	4.42	7.96	NaN	NaN
550	1.29	1.44	1.64	1.91	2.31	2.98	4.23	7.60	NaN	NaN	NaN
500	1.38	1.57	1.83	2.21	2.84	4.04	7.24	NaN	NaN	NaN	NaN
450	1.50	1.75	2.11	2.70	3.84	6.88	NaN	NaN	NaN	NaN	NaN
400	1.67	2.01	2.57	3.63	6.44	NaN	NaN	NaN	NaN	NaN	NaN

(b)

Fig. 5. Simple charging cycle characteristics: (a) Pressure ratio (b) Co-efficient of performance.

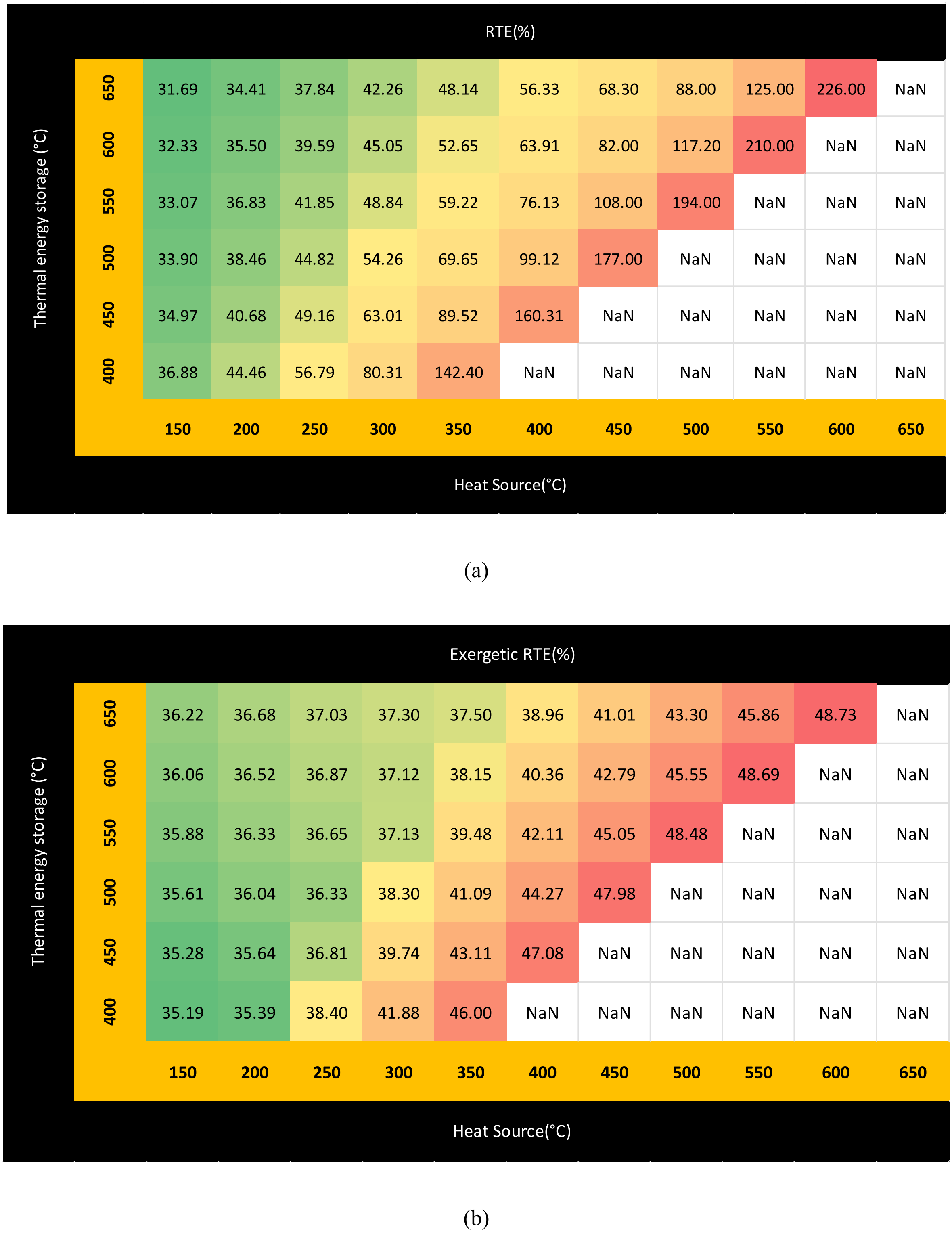

Fig. 6. Performance characteristics of the TI-PTES (a) RTE (b) Exergetic RTE.

As can be seen in Fig. 7, the sCO2 TES HEX outlet temperatures are mapped and are constant for a given storage temperature regardless of the changing HS temperature because the sCO2 inlet and outlet temperatures in TES HEX during charging are dependent on the TES temperature profile, which is independent of the HS temperatures. Hence no change with respect to the HS temperatures can be seen. The configurations where the HS temperature is lower than the sCO2 TES HEX outlet temperature, a recuperator will add the heat to the CO2 stream and elevate the temperature. For example, for the thermal storage temperature of 650 °C, with the HS of 150 °C, a recuperated cycle will elevate the temperature from 150 °C to 359 °C which is 10 °C less than the sCO2 TES HEX outlet temperature and instead of 150 °C, the inlet temperature of the compressor will now become 349 °C which will drastically reduce the required pressure ratio to achieve the temperature of 660 °C for sCO2 to attain the required 650 °C temperature for TES. The combinations that can use the recuperated cycle can be seen on the left side of the

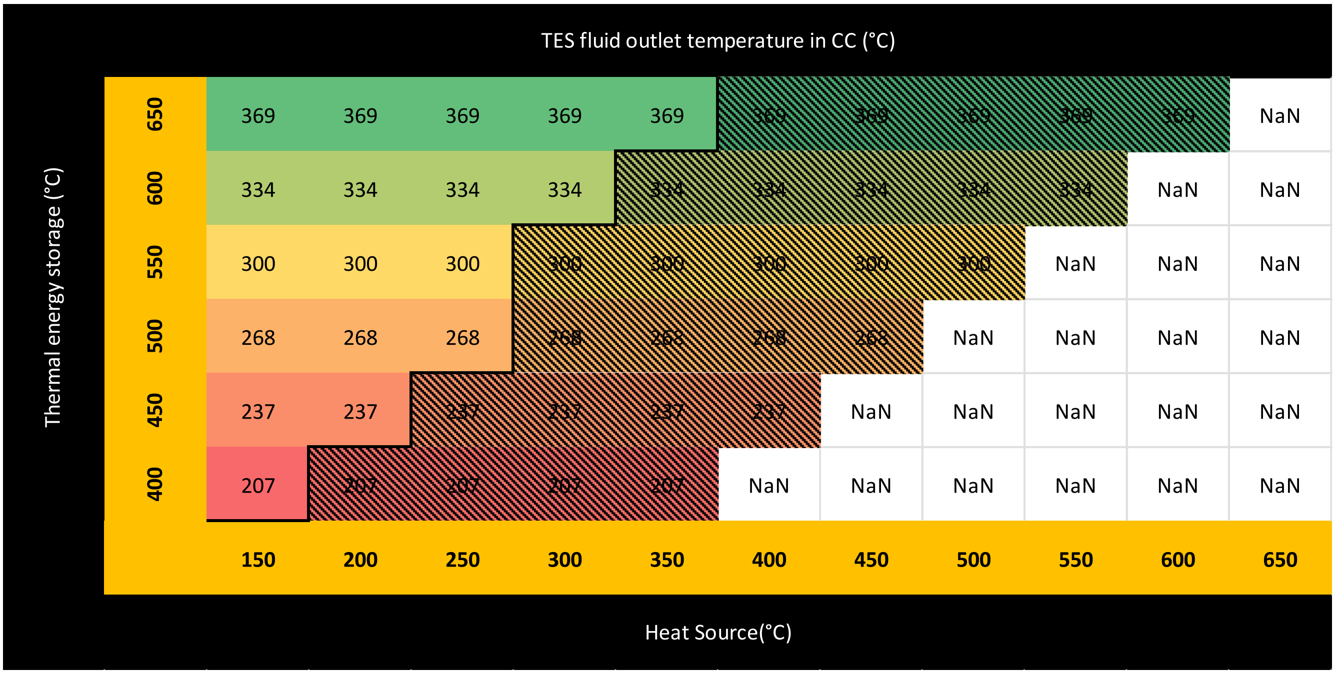

Fig. 7. TI-PTES with the possibility of recuperated charging cycle based on the difference of HS and TES HEX outlet temperature.

border, whereas the combinations that cannot use the recuperated cycle can be seen on the right side of the border with slanted lines. As the temperature gap between the sCO2 from the TES HEX and HS HEX decreases, the recuperated heat will become less. Only those cases in which the recuperation will make sense are included also to account for the economic toll of the recuperator. For example, with 400 °C TES temperature and 200 °C HS temperature the sCO2 TES HEX outlet is 207 °C, the CO2 temperature from the HS HEX is 190 °C and through recuperation the temperature elevation would be 197 °C. Only 7 °C of elevation is not practical enough to add a recuperator to the cycle moreover the pressure ratio for that case is also in satisfactory range even without the recuperator, hence that case has been left out of the recuperated cycles.

Through the recuperation, the pressure ratio has been brought to around 6 and lower which is now a deployable feat for current sCO2 compressors for all the combinations of TES and HS as shown in β CC map in Fig. 8(a). The thick border line separates the combinations of TES and HS using recuperated charging cycle(on the left) overwriting the previous simple charging values at those positions and updating the TES vs HS map. While on the right side we can see the simple charging cycle values now with different color maps than the simple charging cycle. The pressure ratio for the recuperated charging cycle is constant for a particular TES temperature regardless of the HS the CC is coupled to. It is because the compressor inlet conditions in this case are dependent on the sCO2 TES HEX outlet temperature and not on the HS temperature as was in the case of simple CC. So as the sCO2 TES HEX temperature remains constant as we saw in Fig. 7, so does the compressor inlet conditions and hence the pressure ratio for the recuperated cycles.

Unlike the β CC which is constant for a single TES temperature, the COP for the recuperated cycles follows a similar trend to that of the COP of the simple charging cycles where the larger temperature gap between the storage temperature and the HS temperature leads to a smaller COP as shown in Fig. 8(b). However, when comparing the recuperated charging cycles configuration to simple charging cycle counterparts for same TES and HS combination, a visible improvement of COP for the recuperated charging cycles can be seen. For the 650 °C TES temperature and 150 °C HS temperature, the COP has changed from 1.16 to 1.42 which is around 23 % improvement for the least COP case of the simple charging cycle. As the improvement in RTE is largely influenced by the improvement in the COP, the RTE also shows the similar improvement for the case of 650 °C TES and 150 °C HS as it did for the COP as shown in Fig. 9 (a). However, the improvements of the exergetic RTE for the same case is 18.5 % as can be seen in Fig. 9 (b). It is because unlike RTE, exergetic RTE doesn't only depend on the COP but also the destruction of exergy when it gets passed through the extra component, in this case a recuperator. Although the exergetic destruction in the recuperator is less than that of turbomachinery with large pressure ratios as was the case in the simple CC, it is still accounted for, as pointed out in terms of a leaner improvement that we got for the exergetic efficiency for recuperated CC case over simple CC case, as compared to electric RTE. The overall trend of both the RTEs remains the same.

If we single out a case of TES temperature i.e. 650 °C with changing HS temperatures, DC remains the same as TES is the same, the charging cycle however, morphs as the HS changes as can be seen in Appendix C. As the heat source temperature increases, first the recuperation decreases at constant pressure ratio, then the pressure ratio becomes smaller as the higher HS temperature is evaluated for the 650 °C TES. Similarly, heat transfer characteristics of the heat exchangers can also be seen in Appendix C.

4.2. Plant size thermo-economics

After the thermodynamics of TI-PTES configurations, for the preliminary thermo-economic evaluation of the actual plant size, constraints are set to make the comparison viable.

The comparison is made for a fixed amount of power flexibility provided to the grid i.e. electricity taken during CC and released during DC is10 MW (10 MW net power taken from the grid during CC and 10 MW net power that will be provided to the grid in DC) as shown in Table 7. As the power is fixed for our scale up (contrary to the thermodynamic calculations where the intensive KPIs were shown for TES mass flow rate of 1 kg/s) the mass flow rate of the TES fluid will be different in the CC and DC. The ratio of the mass flow rate of TES fluid in CC to the mass flow rate of the TES fluid in DC is shown in Fig. 10(a). The mass flow rate of the TES fluid is higher in DC than in CC for the larger gaps of temperature difference between TES and HS, while the mass flow rate of CC becomes higher as the gap becomes smaller.

While the Fig. 10(b) shows the mass flow ratio of the CO2 in CC to the mass flow rate of the HS showing that lower mass flow rate of HS is

Pressure ratio CC

Thermal energy storage (°C) \ Heat Source(°C)	150	200	250	300	350	400	450	500	550	600	650
650	6.06	6.06	6.06	6.06	6.06	4.56	3.27	2.39	1.79	1.36	NaN
600	5.89	5.89	5.89	5.89	4.92	3.46	2.49	1.83	1.38	NaN	NaN
550	5.70	5.70	5.70	5.35	3.68	2.60	1.89	1.40	NaN	NaN	NaN
500	5.41	5.41	5.41	3.94	2.73	1.94	1.42	NaN	NaN	NaN	NaN
450	5.13	5.13	4.26	2.88	2.01	1.44	NaN	NaN	NaN	NaN	NaN
400	4.79	4.70	3.09	2.11	1.48	NaN	NaN	NaN	NaN	NaN	NaN

(a)

COP

Thermal energy storage (°C) \ Heat Source(°C)	150	200	250	300	350	400	450	500	550	600	650
650	1.42	1.50	1.59	1.69	1.79	2.07	2.50	3.23	4.61	8.30	NaN
600	1.47	1.56	1.66	1.77	1.99	2.41	3.10	4.42	7.96	NaN	NaN
550	1.53	1.63	1.75	1.91	2.31	2.98	4.23	7.60	NaN	NaN	NaN
500	1.60	1.72	1.86	2.21	2.84	4.04	7.24	NaN	NaN	NaN	NaN
450	1.70	1.84	2.11	2.70	3.84	6.88	NaN	NaN	NaN	NaN	NaN
400	1.83	2.01	2.57	3.63	6.44	NaN	NaN	NaN	NaN	NaN	NaN

(b)

Fig 8. Recuperated charging cycle characteristics (a) CC pressure ratio (b) COP.

required for smaller gaps of temperature difference between TES and HS, while the lower absolute temperature values of the TES and HS require lower mass flow rate than the higher absolute temperature values for the equal temperature gaps.

As the mass flow rate of TES in CC and DC vary to compensate the power flexibility of 10 MW. Stored energy during charging and discharging will vary for that amount of power consumption and generation constraints. To have an equal amount of heat stored and released in one complete cycle of this TI-Carnot battery, the time of charging and discharging will vary. Fig. 11 shows the storage as well the time of DC

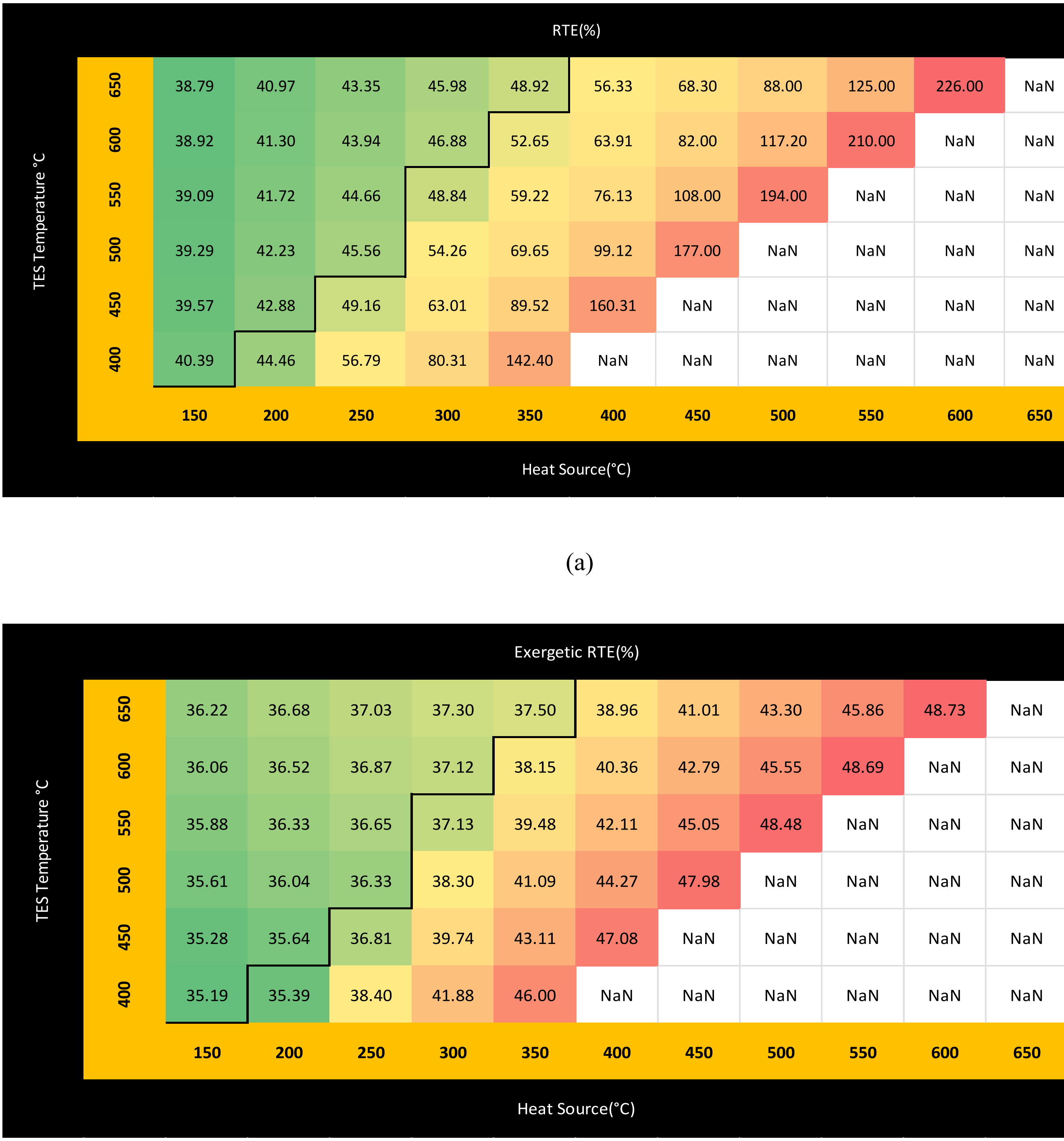

(b)

Fig. 9. Performance characteristics of TI-PTES with recuperated charging (a) RTE (b) Exergetic RTE.

Table 7
Assumption for TI-PTES plant size.

Parameter	Value	UoM
CC Net power intake	10	MW
DC net power generation	10	MW
Charging Time	10	h

for a constant time of 10 h of CC. For a value of HS temperature, the size of the storage gets smaller as the TES temperature becomes higher as can be seen in Fig. 11(a). Less mass flow rate of TES is required to be stored to achieve the required power consumption or generation of 10 MW as the TES temperature gets higher. In other words, lower scaling is needed if higher temperature of storage is selected. If the situation is analyzed from the HS point of view, for a fixed TES temperature, lower HS temperature leads to a smaller storage as well, because lower HS temperature will lead to higher power consumption in the CC for a given TES

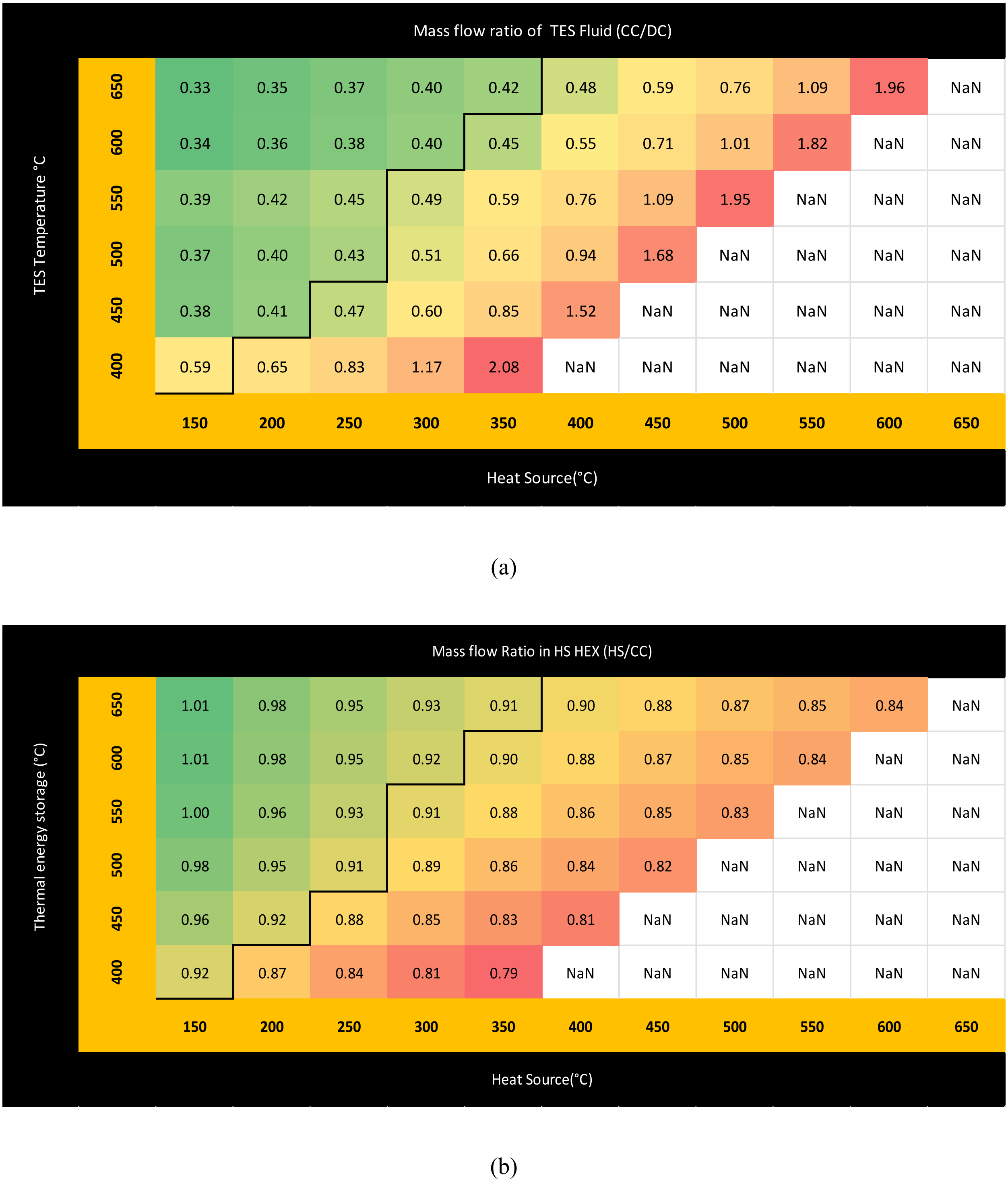

Fig. 10. Mass flow ratios: (a) mass flow CC TES/mass flow DC TES (b) mass flow CC CO2 / mass flow HS.

temperature and mass flow rate, leading again to a smaller scaling value for 10 MW consumption in the charging cycle as compared to the higher HS temperatures which consume smaller values of power to achieve the same results of TES storage. Eventually, the largest amount of storage is required for the smallest temperature gaps between the TES temperature and the HS temperature, while for the same temperature gaps, the amount of energy stored would be higher for smaller absolute values of TES and HS. Fig. 11(b) shows the discharging time of the systems for a fixed charging time of 10 h. As the power flexibility is fixed as well as the storage, the change in energy consumed in CC and energy provided in DC will fall on the time of charging and discharging. With charging time fixed, the discharging time is variable, for 10 h of charging for TI-PTES case of TES 650 °C and HS 150 °C, the discharging can occur for only 3 h and 20 min because of the RTE of the system for the specific coupling case of TI-PTES, whereas for the case of TES 400 °C and HS 350 °C, with 10 h of charging 20 h and 48 min of discharging can be carried out which in turn is based on the RTE of that TI-PTES. From practical point of view, equal amount of grid flexibility such as 10 MW for this case, the application of variable time of charging and discharging that can be achieved for certain TI-PTES configurations can be of interest depending on the

STORAGE (MWh)

Thermal energy storage (°C) \ Heat Source(°C)	150	200	250	300	350	400	450	500	550	600	650
650	14.23	15.03	15.90	16.87	17.94	20.60	25.07	32.32	46.17	83.15	NaN
600	14.69	15.59	16.59	17.70	19.87	24.13	31.01	44.25	79.60	NaN	NaN
550	15.31	16.34	17.50	19.08	23.14	29.75	42.42	76.21	NaN	NaN	NaN
500	16.01	17.20	18.56	22.10	28.38	40.39	72.45	NaN	NaN	NaN	NaN
450	16.98	18.40	21.10	27.04	38.42	68.80	NaN	NaN	NaN	NaN	NaN
400	26.65	29.35	37.50	53.03	94.04	NaN	NaN	NaN	NaN	NaN	NaN

(a)

Discharging Hours (h)

Thermal energy storage (°C) \ Heat Source(°C)	150	200	250	300	350	400	450	500	550	600	650
650	3.34	3.53	3.73	3.96	4.21	4.85	5.90	7.60	10.86	19.57	NaN
600	3.36	3.57	3.79	4.05	4.53	5.50	7.09	10.11	18.19	NaN	NaN
550	3.92	4.18	4.48	4.88	5.92	7.61	10.85	19.50	NaN	NaN	NaN
500	3.73	4.01	4.33	5.14	6.59	9.38	16.83	NaN	NaN	NaN	NaN
450	3.76	4.07	4.67	5.98	8.50	15.23	NaN	NaN	NaN	NaN	NaN
400	5.89	6.49	8.29	11.73	20.80	NaN	NaN	NaN	NaN	NaN	NaN

(b)

Fig. 11. Storage characteristics (a) Required energy storage capacity (b) Discharging hours.

electric market needs. For markets with large hours spans of negative prices may be it is beneficial for going higher charging time configurations and lower discharging time configurations, and vice versa for the markets where the negative or low electricity prices are rare.

4.2.1. Total cost

Fig. 12 shows the total cost of the TI-PTES configurations in the scale of millions. The total cost is between 30 M$ and 65 M$, and is based on many factors other than the TES-HS temperature values. Therefore, we can see no general trend in the capital cost of the TI-PTES but groups. One of the major factors that influence the capital cost is the TES

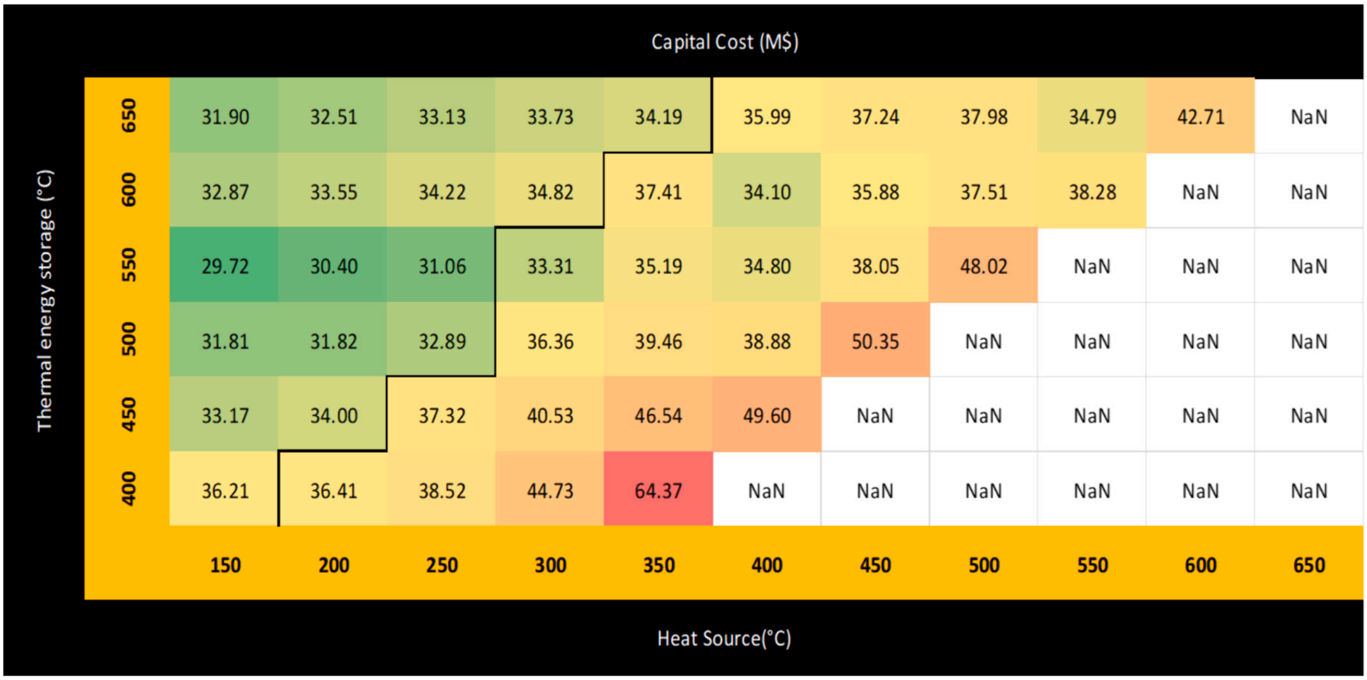

Fig. 12. Capital cost of TI-PTES.

material cost which is different given the material used for the specified storage temperature, The storage material doesn't follow any specific trend of increased or decreased price based on the temperature of storage. However, note that larger the size of TES for a given TI- PTES configuration, greater will be the influence of the TES material factor in the total cost. Other factor influencing the randomization of the capital cost is the size of TES HEX and mass of TES itself. As the mass flow rate of the storage in the charging and discharging are different because of the constant power constraint of 10 MW, the consequent scaling leads to different TES HEX and mass of storage values in charging and discharging. However, in practice, only one TES storage and TES HEX is required for the TI-PTES. Therefore, among CC and DC, the larger size is chosen for the calculation of capital cost which in turn means the costlier among the two; which makes sense from the design point of view because the TES that can support the larger mass flow can certainly support the smaller mass flows as well which is not the case vice versa.

The percentage contribution of the components to the total cost is shown in Fig. 13 has the charging and discharging columns. The storage material as well as TES HEX are shared entities of CC as well as DC. The amount of storage material remains the same for CC and DC, the time to charge and discharge it however can change based on the mass flow rate of the TES fluid acquired from scaling of 10 MW plant. The TES HEX cost determination is however a different scenario, since it is shared by both the CC and DC, there has to be a single TES HEX, however, the temperatures as well as mass flow rates of sCO2 in CC and DC are different. For example, when determining the cost for TES HEX for 650 °C and HS 150 °C PTES, TES HEX for which the UA parameter (on which the cost is based) is larger for discharging as the temperature difference between the hot and the cold side is quite smaller as can be seen in Appendix C.2, the cost of TES HEX is higher in DC so this cost will be used to calculate the TI PTES capex. It is obvious from the Fig. 13 that TES material as well as the TES HEX are the major contributors to the total cost, together with the CC compressor and DC turbine with red and yellow shades for the most configurations, the figure presents an easy way to understand the contribution to the total cost as well as calculate the cost of the individual component by multiplying the contribution factor with the total cost.

4.2.2. *Specific cost*

Following the capital cost and the component contribution analysis, it can be interesting for the designer to know the specific cost of storage as well as power generation. The specific cost maps based on Eqs. 9 and 10 can be seen in Fig. 14. Specific cost of storage is higher for the larger temperature gaps, between the TES and the HS as shown in Fig. 14(a), meaning that for 1 watt-hour of energy stored, larger temperature gaps between the storage and the HS will cost more than the ones with lower temperature gaps between the TES and HS. The values however do not follow a straightforward trend where some specific costs can be seen to be higher for even smaller gaps than the larger gaps for certain TI-PTES configurations that is because the cost as well as the energy stored is influenced by the properties of the TES fluid. There is, however, a general trend which is apparent by the color distribution of the map. From (a), it can be understood that for specific cost required for the storage, CC compressor and the CC recuperator is the force that is driving the specific cost higher for the larger gaps. For larger gaps of TES and HS, higher CC compressor cost incurs. Although in terms of operation, CC recuperator supports the work of the CC compressor, it doesn't provide any support in terms of cost. As the cost of the compressor that might have been decreased because of constant pressure ratios is contributed by the recuperator, so as the temperature gap between the TES and HS is higher so is the recuperation leading to a higher recuperator cost which in turn leads to a higher specific cost of storage for higher temperature gaps, as the temperature gap between TES and HS becomes smaller, so does the recuperator size, the cost of the recuperator and the specific cost of storage.

Similar to the specific cost of storage, specific cost of power generation for the total time of discharging does not follow any general trend as can also be seen in Fig. 14(b). This behavior may not be directly influenced by the TES properties, it is however indirectly influencing in form of discharge cycle capital cost as well as the discharging time. The specific cost of power generation depends on three factors: Power generated which is 10 MW constant, the cost of TES HEX and TES storage are included in the capital cost, whereas the discharging hours also based on the heat stored in TES. In comparison to specific cost of storage, the specific cost of power generation in (b) can generally be attributed to the discharge time of the working fluid in the DC cycle.

Thermal Energy Storage

HS ↓	TES →	400	450	500	550	600	650
150	HEX	20.0%	30.4%	30.3%	29.8%	32.8%	33.0%
	Material	28.5%	15.5%	15.2%	13.5%	12.1%	11.5%
200	HEX	19.9%	29.7%	30.3%	29.1%	32.1%	32.4%
	Material	28.3%	16.4%	15.2%	14.0%	12.6%	11.9%
250	HEX	18.8%	27.0%	29.3%	28.5%	31.5%	31.8%
	Material	31.4%	23.5%	15.9%	14.7%	13.2%	12.3%
300	HEX	16.2%	24.9%	26.6%	26.7%	31.0%	31.2%
	Material	39.6%	28.8%	23.5%	20.2%	13.8%	12.8%
350	HEX	17.0%	21.7%	24.5%	25.2%	28.9%	30.8%
	Material	50.1%	36.6%	28.6%	23.8%	19.5%	13.5%
400	HEX		27.0%	27.6%	28.4%	32.0%	32.5%
	Material		26.3%	17.6%	13.2%	10.1%	8.4%
450	HEX			27.7%	25.9%	30.3%	31.4%
	Material			26.6%	18.7%	13.4%	10.7%
500	HEX				30.4%	29.0%	30.7%
	Material				22.0%	15.1%	11.2%
550	HEX					39.7%	33.6%
	Material					0.8%	0.5%
600	HEX						40.7%
	Material						0.8%

Charging

HS ↓	TES →	400	450	500	550	600	650
150	COMP	19.2%	20.7%	21.3%	22.6%	22.4%	22.9%
	RECUP	1.3%	1.6%	1.8%	2.0%	2.1%	2.2%
	TURB	3.4%	3.6%	3.5%	3.6%	3.4%	3.4%
	HS HEX	2.1%	2.0%	1.8%	1.8%	1.6%	1.5%
200	COMP	18.7%	19.8%	20.9%	21.7%	21.4%	22.0%
	RECUP		1.0%	1.8%	1.8%	1.9%	2.1%
	TURB	4.2%	4.2%	4.2%	4.2%	3.9%	3.9%
	HS HEX	2.6%	2.4%	2.3%	2.1%	1.9%	1.8%
250	COMP	17.6%	18.4%	20.9%	21.8%	21.5%	22.0%
	RECUP			0.5%	1.3%	1.6%	1.9%
	TURB	3.9%	4.2%	4.8%	4.8%	4.5%	4.4%
	HS HEX	3.4%	2.7%	2.5%	2.4%	2.2%	2.0%
300	COMP	15.1%	16.9%	18.9%	20.8%	21.7%	22.2%
	RECUP					0.9%	1.5%
	TURB	3.3%	3.8%	4.4%	5.0%	5.1%	4.9%
	HS HEX	4.4%	3.5%	3.0%	2.6%	2.4%	2.3%
350	COMP	10.5%	14.6%	17.4%	19.6%	20.5%	22.4%
	RECUP						0.5%
	TURB	2.3%	3.3%	4.0%	4.7%	5.0%	5.5%
	HS HEX	5.2%	4.4%	3.8%	3.3%	2.7%	2.5%
400	COMP		15.2%	19.6%	22.0%	22.6%	23.7%
	RECUP						
	TURB		3.4%	4.5%	5.2%	5.4%	5.9%
	HS HEX		8.0%	6.2%	5.0%	3.9%	3.3%
450	COMP			15.1%	20.1%	21.4%	22.9%
	RECUP						
	TURB			3.4%	4.7%	5.2%	5.6%
	HS HEX			8.2%	6.6%	5.1%	4.2%
500	COMP				15.9%	20.5%	22.4%
	RECUP						
	TURB				3.7%	4.9%	5.5%
	HS HEX				9.0%	7.0%	5.5%
550	COMP					20.0%	24.3%
	RECUP						
	TURB					4.7%	5.9%
	HS HEX					11.7%	8.7%
600	COMP						19.8%
	RECUP						
	TURB						4.7%
	HS HEX						12.0%

Discharging

HS ↓	TES	400	450	500	550	600	650
150	COMP	12.0%	12.2%	12.2%	12.5%	12.0%	12.0%
	RECUP	2.6%	2.7%	2.6%	2.6%	2.4%	1.4%
	TURB	8.9%	9.3%	9.4%	9.9%	9.7%	9.8%
	CL HEX	2.0%	1.9%	1.7%	1.7%	1.4%	1.3%
200	COMP	11.9%	11.9%	12.2%	12.3%	11.8%	11.8%
	RECUP	2.6%	2.6%	2.6%	2.5%	2.4%	2.3%
	TURB	8.8%	9.1%	9.4%	9.7%	9.5%	9.6%
	CL HEX	2.9%	2.8%	2.7%	2.6%	2.4%	2.3%
250	COMP	11.3%	10.9%	11.8%	12.0%	11.6%	11.6%
	RECUP	2.5%	2.4%	2.5%	2.5%	2.3%	2.3%
	TURB	8.4%	8.3%	9.1%	9.5%	9.3%	9.4%
	CL HEX	2.8%	2.6%	2.6%	2.5%	2.3%	2.2%
300	COMP	9.7%	10.0%	10.7%	11.2%	11.4%	11.4%
	RECUP	2.1%	2.2%	2.3%	2.3%	2.3%	2.2%
	TURB	7.2%	7.6%	8.3%	8.8%	9.1%	9.3%
	CL HEX	2.4%	2.4%	2.4%	2.4%	2.3%	2.2%
350	COMP	6.7%	8.7%	9.8%	10.6%	10.6%	11.2%
	RECUP	1.5%	1.9%	2.1%	2.2%	2.1%	2.2%
	TURB	5.0%	6.6%	7.6%	8.3%	8.5%	9.1%
	CL HEX	1.7%	2.1%	2.2%	2.2%	2.1%	2.2%
400	COMP		9.1%	11.1%	11.9%	11.7%	11.8%
	RECUP		2.0%	2.3%	2.4%	2.4%	2.3%
	TURB		6.9%	8.6%	9.4%	9.4%	9.6%
	CL HEX		2.2%	2.5%	2.5%	2.4%	2.3%
450	COMP			8.6%	10.9%	11.1%	11.4%
	RECUP			1.8%	2.2%	2.2%	2.3%
	TURB			6.6%	8.6%	8.9%	9.3%
	CL HEX			2.2%	2.5%	2.4%	2.3%
500	COMP				8.6%	10.6%	11.2%
	RECUP				1.8%	2.1%	2.2%
	TURB				6.8%	8.5%	9.1%
	CL HEX				1.8%	2.2%	2.2%
550	COMP					10.4%	12.2%
	RECUP					2.1%	2.4%
	TURB					8.4%	10.0%
	CL HEX					2.1%	2.4%
600	COMP						10.0%
	RECUP						2.0%
	TURB						8.1%
	CL HEX						1.9%

Fig. 13. Component contributions in the capital cost.

Specific Cost of Storage ($/Wh)

Thermal energy storage (°C) \ Heat Source(°C)	150	200	250	300	350	400	450	500	550	600	650
650	1.65	1.60	1.55	1.50	1.43	1.29	1.11	0.88	0.55	0.40	NaN
600	1.64	1.59	1.54	1.47	1.04	0.98	0.87	0.65	0.37	NaN	NaN
550	1.41	1.36	1.31	1.31	1.17	0.86	0.68	0.51	NaN	NaN	NaN
500	1.45	1.35	1.31	1.26	1.09	0.73	0.56	NaN	NaN	NaN	NaN
450	1.42	1.36	1.34	1.17	0.98	0.58	NaN	NaN	NaN	NaN	NaN
400	0.99	0.91	0.77	0.66	0.58	NaN	NaN	NaN	NaN	NaN	NaN

(a)

Specific Cost of Power Generation ($/Wh)

Thermal energy storage (°C) \ Heat Source(°C)	150	200	250	300	350	400	450	500	550	600	650
650	0.90	0.85	0.86	0.97	1.39	0.98	0.81	0.56	0.28	0.13	NaN
600	0.80	0.77	0.82	0.84	0.89	0.69	0.49	0.31	0.16	NaN	NaN
550	0.65	0.61	0.58	0.61	0.55	0.42	0.28	0.15	NaN	NaN	NaN
500	0.63	0.59	0.56	0.52	0.43	0.31	0.17	NaN	NaN	NaN	NaN
450	0.63	0.59	0.52	0.41	0.32	0.18	NaN	NaN	NaN	NaN	NaN
400	0.39	0.36	0.28	0.20	0.11	NaN	NaN	NaN	NaN	NaN	NaN

(b)

Fig. 14. Specific cost (a) Storage (b) Power generation.

Because unlike CC, DC pressure ratio is fixed, the capital cost causes some anomalies based on the TES HEX and material selection but the general trend shows lower specific costs for combinations that lead to higher discharging hours.

Over all, it can be interesting to find the TI-PTES configuration which is optimized for specific costs of storage as well as power generation for a given application leading to a cost effective solution.

The results discussed in the study provide a comprehensive understanding of the role that freely available heat sources can play in uplifting the performance of the pumped thermal energy systems. Different heat sources are explored for different options of storages which can be selected for appropriate application required. Heat coming from industrial waste heat of low grade which is not easily exploitable through power cycles can be one of the main beneficiaries of this type of technology, more higher temperature heat sources from renewables such as solar thermal and biomass can also be valorized nonetheless and may be more beneficial to be exploited in supporting CC at times of peak shaving. The mapping contains some configurations with as low as 50 °C HS-TES temperature, which may beg the question that why not utilize the source directly for power generation instead of using it for storage at a mere 50 °C higher temperature. The counter argument is that the added value of the heat source in this type of technology is to support the storage of surplus electricity already present in the market, by lowering the isentropic losses of the turbomachinery in the charging by elevating the temperatures above the ambient to that of the heat source thus increasing the roundtrip efficiency. The generation of electricity using the heat source on the other hand, in the market at the time when it is brimming with surplus energy is just illogical. On the other hand, storing the energy with the temperature gap as low as 50 °C has its drawbacks in terms of large size of machinery required to compensate for the large mass flow rate to provide the same amount of grid power flexibility as can be provided by the configuration with 300 °C of temperature gap with the lower round trip efficiency however. For each application, therefore, it is crucial to find the right balance between the performance as well as the cost when considering the TES for available heat source for a TI-PTES system.

5. Conclusion

This study presents modelling results (achieved via a novel tool named WTEMP-EVO developed by the authors) through a mapping technique, the utilization of freely available heat sources for the purpose of valorizing them via sCO_2 based thermally integrated pumped thermal energy storage(TI-PTES). Heat sources from 150 °C to 600 °C are evaluated for this purpose supporting the commercially available high temperature storages 400 °C to 650 °C. 45 configurations of TI-PTES have been studied each utilizing a unique combination of heat source temperature and a thermal storage temperature. The study finds that:

- For larger temperature gaps between HS and TES, COP for the charging cycle gets lower, whereas the thermal efficiency of the discharging cycle gets higher. The RTE, however gets lower as it is influenced more by the charging cycle COP. For smaller temperature differences between HS-TES, RTE can get>100 % for certain configurations. The exergetic round trip efficiency follows the similar trend
- Both simple and recuperated charging configurations have their benefits and short comings. The former is constrained by turbomachinery technology and cost for very large pressure ratios, however it is thermodynamically possible for all the combinations of heat source and storage temperature. Latter configuration although reduces the pressure ratio, increases the RTE, the recuperation however is not thermodynamically possible for all the combinations.
- For a fixed grid flexibility (10 MW charging and discharging), the mass flow rates consequently the cost of equipment for smaller gaps of heat sources and storage temperatures becomes really high and vice versa, so from the economical point of view it makes sense to use large temperature gap combinations. On the other hand, the RTE consequently the discharging time of the combinations with large temperature gap is really low and vice versa. So for each individual application, a tradeoff is to be expected between cost and performance.
- The capital cost of the TI-PTES combinations is largely influenced by the material of the thermal energy storage used. Since the material cost is not proportional to the temperature of utilization, the capital cost doesn't show trend of changing storage temperatures.
- The specific cost of energy storage through charging and energy retrieval through power generation show higher cost/Wh for larger temperature gaps. The specific cost of power generation however is smaller than that of storage, showing the economic toll charging component has on the TI-PTES despite the thermal integration support. Higher the thermal support relative to the storage, lower is the specific cost of charging.

The results of the study show (at many different HS-TES temperature levels) the relevance of sCO2 based TI-PTES from the RTE point of view of the system, particularly if compared with other competing state of the art/currently investigated LDES and energy storage solutions while CAPEX of the proposed system (compared for a 10 MW/10^2 MWh capacity) are also comparable with other LDES technologies as reported in Table 8 [17,65–67]. Despite being at a really early development stages sCO2 TI-PTES show great promise for LDES applications of grid flexibility while being highly competitive from both RTE as well as CAPEX point of view to electrochemical batteries (battery CAPEX are usually evaluated for lower duration/scales and cannot yet be termed as LDES), that boast the highest RTE values. But thanks to the heat integrating nature of PTES, that it can boast RTE >100 %.

This study only covers the basic configurations of the charging and discharging cycles in order to evaluate large set of storage and heat source combinations. For a given case study, configurations can be further improved to get better performances, sometimes at the expense of complex cycles and elevated costs. The RTE used for this case is a thermodynamic RTE, that assumes back to back charging and discharging cycles. However in real case scenarios, the power components might be idle for hours and the energy stored may be subjected to degradation of state of charge, therefore, thermal losses should also be considered as a relevant parameter of the thermal energy storage materials for future studies. Following the detailed TI-PTES maps for heat source utilization, evaluation of the thermo-economic performances in terms of LCOS for different heat source case studies in different EU electric markets can be the next steps in practical implementation of sCO2 TI PTES.

CRediT authorship contribution statement

Syed Safeer Mehdi Shamsi: Writing – review & editing, Writing – original draft, Software, Methodology, Formal analysis, Conceptualization. **Stefano Barberis:** Writing – original draft, Supervision, Resources, Project administration, Funding acquisition. **Simone Maccarini:** Software, Methodology. **Alberto Traverso:** Writing – review & editing, Supervision, Resources, Project administration, Funding acquisition.

Declaration of competing interest

The authors declare that they have no known competing financial interests or personal relationships that could have appeared to influence the work reported in this paper.

Data availability

two files for simple and recuperated charging cycles have been

Table 8
Benchmark of proposed sCO2 TI-PTES and other LDES/energy storage solutions.[1]

Energy storage solution	RTE [%]	CAPEX [$/kWh]	TRL
Proposed sCO2 TI-PTES[2]	30–220	7–429	4
Pumped hydro	80–85	5–200	9
CAES	50–65	2–120	8
LAES	70–85	300–600	7
Batteries	85–95	400–3800	9

[1] Storage technology($/kWh) and not the power generating technology ($/kW) are compared for fair comparison.
[2] Depending on the HS-TES temperature.

shared showing the charging cycle thermodynamic properties

Acknowledgements

This work has been partially funded by the European Union in the Horizon Europe framework under Grant Agreement n. 10113600. Views and opinions expressed are however those of the author(s) only and do not necessarily reflect those of the European Union or of the European Climate, Infrastructure and Environment Executive Agency (CINEA). Neither the European Union nor the granting authority can be held responsible for them.

The work presented here has also been partially supported by the Italian National project PRIN 2022 "ECO-Sustainable cost-Effective CO2 cycles tArgeting Renewable dispatCHable powER and Storage" (ECO-SEARCHERS).

Appendix A. Supplementary data

Supplementary data to this article can be found online at https://doi.org/10.1016/j.est.2024.112979.

Appendix B

B.1. Cost functions for components

CC/DC compressor	$1230000 \times Compressor\ Power^{0.3992}$ If $\begin{cases} p_{Out} = 245\ bar\ to\ 345\ bar \\ p_{in} = 65\ bar\ to\ 90\ bar \end{cases}$	Wieland [68]
	$160000 \times Compressor\ Power^{0.8} \times f_t \times f_P$ $f_t = \begin{cases} 1\ if\ T_{max} < 673\ K \\ 5.32 - 0.0238 \times T_{max}(^\circ C) + 0.00003 \times {T_{max}}^2(^\circ C)\ if\ T_{max} \geq 673\ K \end{cases}$ $f_P = \begin{cases} 1\ if\ P_{max} < 10\ MPa \\ 0.8 + 0.02 \times P_{max}(^\circ C) + 0.00003 \times {T_{max}}^2(^\circ C)\ if\ P_{max} \geq 10\ Mpa \end{cases}$	Zhao [69]
	$1230000 \times Compressor\ Power^{0.3992} \times f_t \times f_P$ $f_t = \begin{cases} 1\ if\ T_{max} < 673\ K \\ 5.32 - 0.0238 \times T_{max}(^\circ C) + 0.00003 \times {T_{max}}^2(^\circ C)\ if\ T_{max} \geq 673\ K \end{cases}$ $f_P = \begin{cases} 1\ if\ P_{max} < 10\ MPa \\ 0.8 + 0.02 \times P_{max}(^\circ C) + 0.00003 \times {T_{max}}^2(^\circ C)\ if\ P_{max} \geq 10\ Mpa \end{cases}$	Wieland with Zhao Correction factor
CC/DC turbine	$406200 \times Turbine\ Power^{0.8}\ (Radial)$ If $\begin{cases} Turbine\ Power \geq 1\ MW \\ Turbine\ Power \leq 35\ MW \end{cases}$ $182600 \times Turbine\ Power^{0.5561}\ (Axial)$ If $\begin{cases} Turbine\ Power \geq 10\ MW \\ Turbine\ Power \leq 750\ MW \end{cases}$ $1000 \times (Turbine\ Power \times 1000)^{0.6} \times 1.86\ (Bladeless/tesla\ turbine)$ If { $Turbine\ Power < 1MW$	[68]
Recuperator	$49.45 \times abs(UA)^{0.7544} \times f_T$ $f_t = \begin{cases} 1\ if\ T_{max} < 550^\circ C \\ 1 + 0.02141 \times (T_{max} - 550^\circ C)\ if\ T_{max} \geq 550^\circ C \end{cases}$	[68]
TES HEX	$17.5 \times abs(UA)^{0.8778}$	[70]
HS HEX	$17.5 \times abs(UA)^{0.8778} \times f_T$ $f_t = \begin{cases} 0.8\ if\ T_{max} < 400^\circ C \\ 1\ if\ T_{max} \geq 400^\circ C \end{cases}$	[70]
DC Cooler	$32.88 \times abs(UA)^{0.75}$	[68]
Thermal Energy Storage	For thermal oils and molten salts Cost of Storage material: FRAGOLTHERM-X-75-A Silicon oil, 4 $/kg YARA SALT, 1.5 $/kg HITEC XL, 1.5 $/kg Solar Salt, 1.5 $/kg Solid media/Packed Bed TES: *High Temperature Insulation* 4269 [$/m³] *Low Temperature Insulation* 616 [$/m³] *253 MA Stainless Steel* 42,354 [$/m³] *Natural Rocks* 66 [$/m³] *Foundations* 1210 [$/m²] $TES\ Cost = Mass\ flow\ rate\ of\ TES\ working\ fluid\left(\frac{kg}{s}\right) \times Max\ CC\ orDC\ time(s) \times Cost\ of\ Storage\ material\left(\frac{\$}{kg}\right)$	[60] [61] [62] [59]

Appendix C

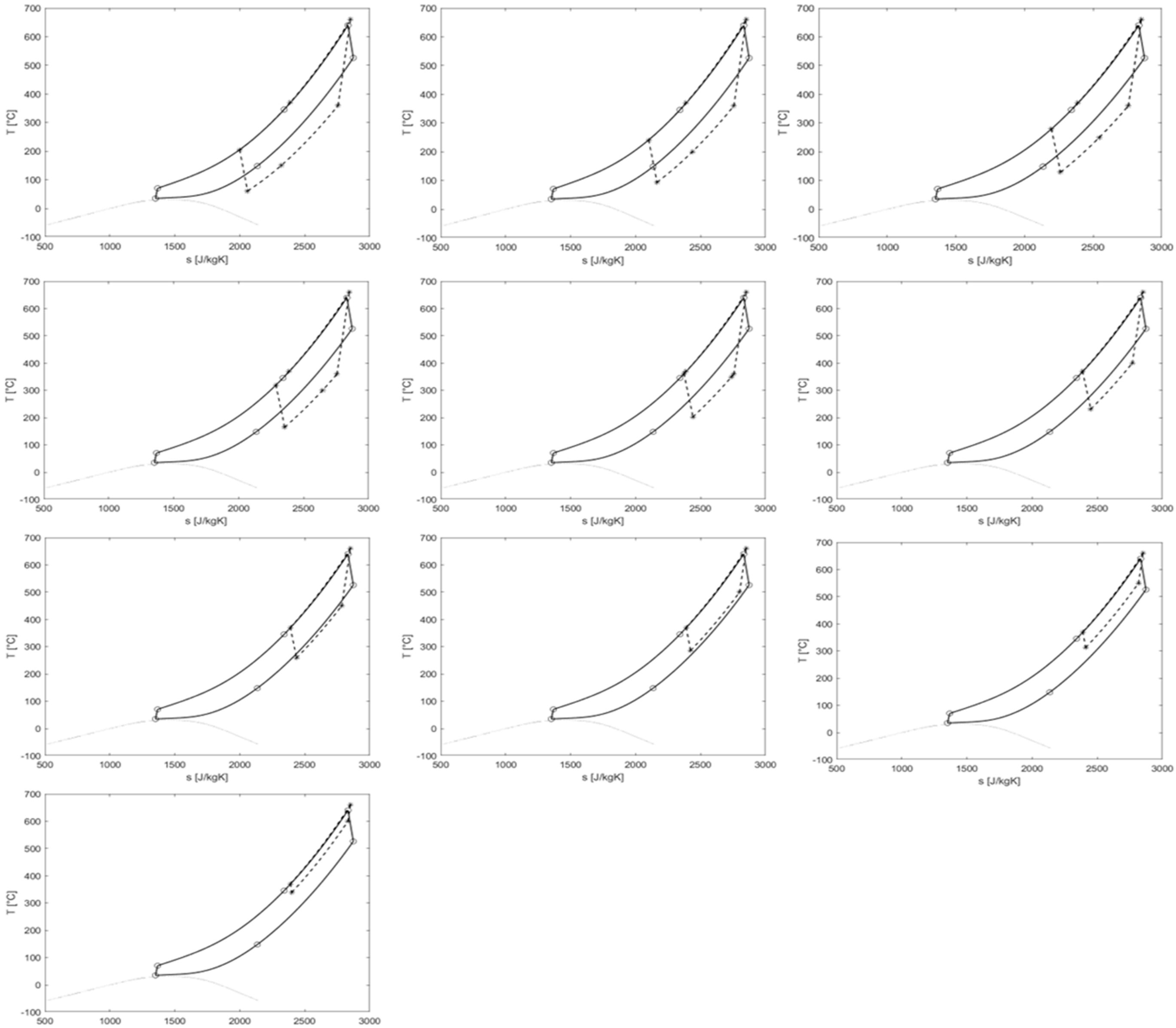

Fig. C.1. TS diagrams of TI-PTES with storage temperature 650 °C and HS variations from 150 °C to 600 °C (from left to right): dotted line shows charging, solid line shows discharging.

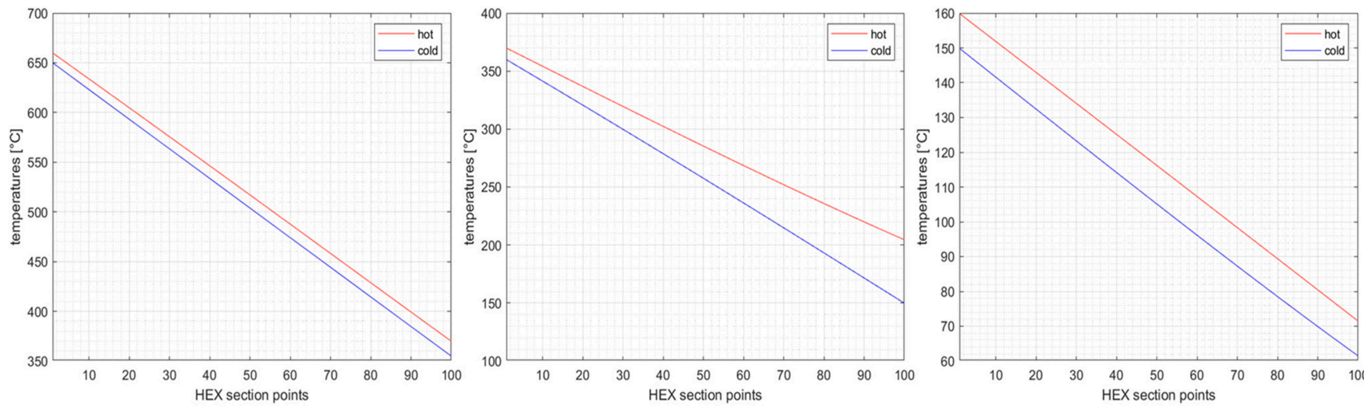

(a)

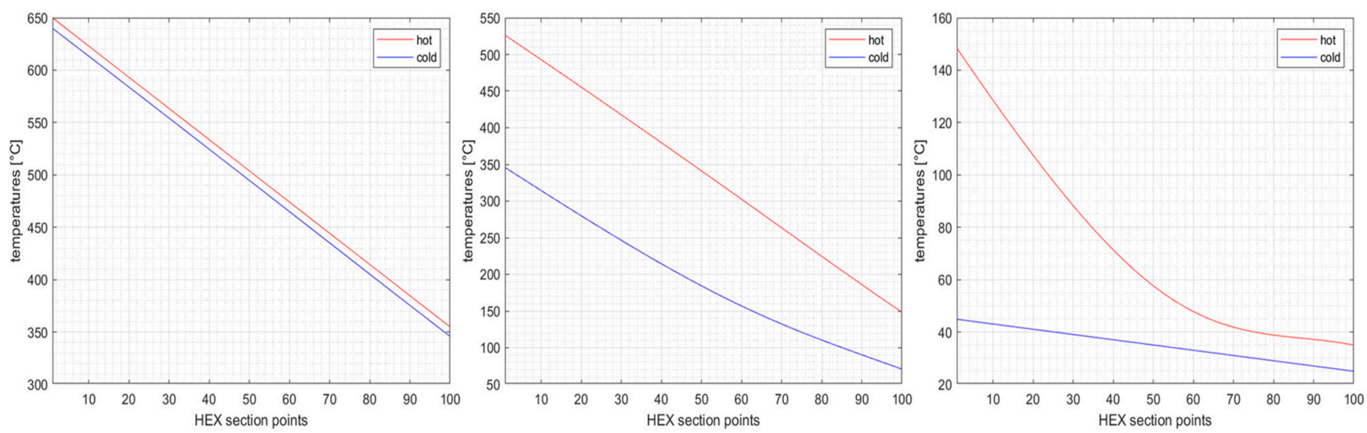

(b)

Fig. C.2. Internal heat transfer characteristics of HEX for TI PTES with TES: 650 °C and HS: 150 °C. Left: TES HEX, Mid: Recuperator, Right: HS HEX/Cooler (a) Charging (b) Discharging

Appendix D

$$p_{Out} = p_{In} \bullet \beta_{Compr} \tag{D1}$$

$$p_{Out} = p_{In} * (1 - \Delta p_{\%Loss}) \tag{D2}$$

$$h_{Out} = h_{In} + \eta_{Turb} \bullet (h_{Out-isoentr} - h_{In}) \tag{D3}$$

$$h_{Out} = h_{In} + (h_{Out-isoentr} - h_{In}) / \eta_{Comp} \tag{D4}$$

$$\varepsilon_{HEX} = Q_{HEX} / Q_{HEX-max} \tag{D5}$$

$$Q_{HEX} = \dot{m}_{cold} * (h_{Out-cold} - h_{In-cold}) \tag{D6}$$

References

[1] M. Amir, et al., Energy storage technologies: an integrated survey of developments, global economical/environmental effects, optimal scheduling model, and sustainable adaption policies, Journal of Energy Storage 72 (Nov. 2023) 108694, https://doi.org/10.1016/j.est.2023.108694.

[2] L. Magistri, P. Costamagna, A.F. Massardo, C. Rodgers, C.F. McDonald, A hybrid system based on a personal turbine (5 kW) and a solid oxide fuel cell stack: a flexible and high efficiency energy concept for the distributed power market, J. Eng. Gas Turbines Power 124 (4) (Sep. 2002) 850–857, https://doi.org/10.1115/1.1473825.

[3] R. Gómez-Calvet, J.M. Martínez-Duart, A.R. Gómez-Calvet, The 2030 power sector transition in Spain: too little storage for so many planned solar photovoltaics? Renew. Sust. Energ. Rev. 174 (Mar. 2023) 113094 https://doi.org/10.1016/j.rser.2022.113094.

[4] W. Wang, B. Yuan, Q. Sun, R. Wennersten, Application of energy storage in integrated energy systems — a solution to fluctuation and uncertainty of renewable energy, Journal of Energy Storage 52 (Aug. 2022) 104812, https://doi.org/10.1016/j.est.2022.104812.
[5] M. Gholami, M.J. Sanjari, A. Berrada, Game theoretical approach for critical sizing of energy storage systems for residential prosumers, Journal of Energy Storage 64 (Aug. 2023) 107166, https://doi.org/10.1016/j.est.2023.107166.
[6] "Progress and prospects of energy storage technology research: based on multidimensional comparison - ScienceDirect." Accessed: Jan. 19, 2024. [Online]. Available: https://www.sciencedirect.com/science/article/pii/S2352152X23031080?via%3Dihub.
[7] A.M. López-Grajales, J.W. González-Sanchez, H.A. Cardona-Restrepo, I.A. Isaac-Millan, G.J. López-Jiménez, O.H. Vasco-Echeverri, Economy, financial, and regulatory method for the integration of electrical energy storage in a power network, Journal of Energy Storage 58 (Feb. 2023) 106433, https://doi.org/10.1016/j.est.2022.106433.
[8] R.S. Gupta, A. Tyagi, S. Anand, Optimal allocation of electric vehicles charging infrastructure, policies and future trends, Journal of Energy Storage 43 (Nov. 2021) 103291, https://doi.org/10.1016/j.est.2021.103291.
[9] B. Krietemeyer, J. Dedrick, E. Sabaghian, T. Rakha, Managing the duck curve: energy culture and participation in local energy management programs in the United States, Energy Res. Soc. Sci. 79 (Sep. 2021) 102055, https://doi.org/10.1016/j.erss.2021.102055.
[10] S. Naderi, et al., Clustering based analysis of residential duck curve mitigation through solar pre-cooling: a case study of Australian housing stock, Renew. Energy 216 (Nov. 2023) 119064, https://doi.org/10.1016/j.renene.2023.119064.
[11] Q. Hou, N. Zhang, E. Du, M. Miao, F. Peng, C. Kang, Probabilistic duck curve in high PV penetration power system: concept, modeling, and empirical analysis in China, Appl. Energy 242 (May 2019) 205–215, https://doi.org/10.1016/j.apenergy.2019.03.067.
[12] A. Giugno, A. Sorce, A. Cuneo, S. Barberis, Effects of market and climatic conditions over a gas turbine combined cycle integrated with a heat pump for inlet cooling, Appl. Energy 290 (May 2021) 116724, https://doi.org/10.1016/j.apenergy.2021.116724.
[13] A. Vannoni, J.A. Garcia, W. Mantilla, R. Guedez, A. Sorce, "Ancillary Services Potential for Flexible Combined Cycles," presented at the ASME Turbo Expo 2021: Turbomachinery technical conference and exposition, American Society of Mechanical Engineers Digital Collection Sep, 2021, https://doi.org/10.1115/GT2021-59587.
[14] O. Kwon, S. Lee, J. Park, A numerical study to compensate duck curve of ESS integrated gas turbine system with reused-battery, Journal of Energy Storage 55 (Nov. 2022) 105422, https://doi.org/10.1016/j.est.2022.105422.
[15] A. Vannoni, A. Giugno, A. Sorce, Integration of a flue gas condensing heat pump within a combined cycle: thermodynamic, environmental and market assessment, Appl. Therm. Eng. 184 (Feb. 2021) 116276, https://doi.org/10.1016/j.applthermaleng.2020.116276.
[16] J. Twitchell, K. DeSomber, D. Bhatnagar, Defining long duration energy storage, Journal of Energy Storage 60 (Apr. 2023) 105787, https://doi.org/10.1016/j.est.2022.105787.
[17] A. Vecchi, A. Sciacovelli, Long-duration thermo-mechanical energy storage – present and future techno-economic competitiveness, Appl. Energy 334 (Mar. 2023) 120628, https://doi.org/10.1016/j.apenergy.2022.120628.
[18] W.-D. Steinmann, Thermo-mechanical concepts for bulk energy storage, Renew. Sust. Energ. Rev. 75 (Aug. 2017) 205–219, https://doi.org/10.1016/j.rser.2016.10.065.
[19] M.A. Hannan, et al., Impact assessment of battery energy storage systems towards achieving sustainable development goals, Journal of Energy Storage 42 (Oct. 2021) 103040, https://doi.org/10.1016/j.est.2021.103040.
[20] Q. Hassan, A.Z. Sameen, H.M. Salman, M. Jaszczur, A.K. Al-Jiboory, Hydrogen energy future: advancements in storage technologies and implications for sustainability, Journal of Energy Storage 72 (Nov. 2023) 108404, https://doi.org/10.1016/j.est.2023.108404.
[21] A. Vannoni, A. Sorce, A. Traverso, A.F. Massardo, Techno-economic analysis of power-to-heat systems, E3S Web Conf. 238 (2021) 03003, https://doi.org/10.1051/e3sconf/202123803003.
[22] L. Scapino, C. De Servi, H.A. Zondag, J. Diriken, C.C.M. Rindt, A. Sciacovelli, Techno-economic optimization of an energy system with sorption thermal energy storage in different energy markets, Appl. Energy 258 (Jan. 2020) 114063, https://doi.org/10.1016/j.apenergy.2019.114063.
[23] S. Trevisan, B. Buchbjerg, R. Guedez, Power-to-heat for the industrial sector: techno-economic assessment of a molten salt-based solution, Energy Convers. Manag. 272 (Nov. 2022) 116362, https://doi.org/10.1016/j.enconman.2022.116362.
[24] M. Raggio, M.L. Ferrari, Compressed air energy storage with T100 microturbines: dynamic analysis and operational constraints, Journal of Energy Storage 73 (Dec. 2023) 109093, https://doi.org/10.1016/j.est.2023.109093.
[25] A. Vecchi, Y. Li, Y. Ding, P. Mancarella, A. Sciacovelli, Liquid air energy storage (LAES): a review on technology state-of-the-art, integration pathways and future perspectives, Advances in Applied Energy 3 (Aug. 2021) 100047, https://doi.org/10.1016/j.adapen.2021.100047.
[26] O. Dumont, G.F. Frate, A. Pillai, S. Lecompte, M. De Paepe, V. Lemort, Carnot battery technology: a state-of-the-art review, Journal of Energy Storage 32 (Dec. 2020) 101756, https://doi.org/10.1016/j.est.2020.101756.
[27] A. Benato, A. Stoppato, Pumped thermal electricity storage: a technology overview, Thermal Science and Engineering Progress 6 (Jun. 2018) 301–315, https://doi.org/10.1016/j.tsep.2018.01.017.
[28] S. Sharma, M. Mortazavi, Pumped thermal energy storage: a review, Int. J. Heat Mass Transf. 213 (Oct. 2023) 124286, https://doi.org/10.1016/j.ijheatmasstransfer.2023.124286.
[29] P. Wang, et al., Comparative analysis of system performance of thermally integrated pumped thermal energy storage systems based on organic flash cycle and organic Rankine cycle, Energy Convers. Manag. 273 (Dec. 2022) 116416, https://doi.org/10.1016/j.enconman.2022.116416.
[30] B. Eppinger, L. Zigan, J. Karl, S. Will, Pumped thermal energy storage with heat pump-ORC-systems: comparison of latent and sensible thermal storages for various fluids, Appl. Energy 280 (Dec. 2020) 115940, https://doi.org/10.1016/j.apenergy.2020.115940.
[31] J.D. McTigue, P. Farres-Antunez, K.S. J, C.N. Markides, A.J. White, Techno-economic analysis of recuperated joule-Brayton pumped thermal energy storage, Energy Convers. Manag. 252 (Jan. 2022) 115016, https://doi.org/10.1016/j.enconman.2021.115016.
[32] W.D. Steinmann, The CHEST (compressed heat energy STorage) concept for facility scale thermo mechanical energy storage, Energy 69 (May 2014) 543–552, https://doi.org/10.1016/j.energy.2014.03.049.
[33] F. Catapano, et al., Development and experimental testing of an integrated prototype based on Stirling, ORC and a latent thermal energy storage system for waste heat recovery in naval application, Appl. Energy 311 (Apr. 2022) 118673, https://doi.org/10.1016/j.apenergy.2022.118673.
[34] M. Nilsson, Simplified pumped thermal energy storage using a two-way Stirling cycle, Journal of Energy Storage 73 (Dec. 2023) 108994, https://doi.org/10.1016/j.est.2023.108994.
[35] S.S.M. Shamsi, S. Barberis, S. Maccarini, A. Traverso, Large scale energy storage systems based on carbon dioxide thermal cycles: a critical review, Renew. Sust. Energ. Rev. 192 (Mar. 2024) 114245, https://doi.org/10.1016/j.rser.2023.114245.
[36] J. Blanquiceth, J.M. Cardemil, M. Henríquez, R. Escobar, Thermodynamic evaluation of a pumped thermal electricity storage system integrated with large-scale thermal power plants, Renew. Sust. Energ. Rev. 175 (Apr. 2023) 113134, https://doi.org/10.1016/j.rser.2022.113134.
[37] G.F. Frate, L. Ferrari, P. Sdringola, U. Desideri, A. Sciacovelli, Thermally integrated pumped thermal energy storage for multi-energy districts: integrated modelling, assessment and comparison with batteries, Journal of Energy Storage 61 (May 2023) 106734, https://doi.org/10.1016/j.est.2023.106734.
[38] K. Ökten, B. Kurşun, Thermo-economic assessment of a thermally integrated pumped thermal energy storage (TI-PTES) system combined with an absorption refrigeration cycle driven by low-grade heat source, Journal of Energy Storage 51 (Jul. 2022) 104486, https://doi.org/10.1016/j.est.2022.104486.
[39] M. Zhang, L. Shi, P. Hu, G. Pei, G. Shu, Carnot battery system integrated with low-grade waste heat recovery: toward high energy storage efficiency, Journal of Energy Storage 57 (Jan. 2023) 106234, https://doi.org/10.1016/j.est.2022.106234.
[40] P. Farres-Antunez, J.D. McTigue, A.J. White, A pumped thermal energy storage cycle with capacity for concentrated solar power integration, in: 2019 Offshore Energy and Storage Summit (OSES) Jul, 2019, pp. 1–10, https://doi.org/10.1109/OSES.2019.8867222.
[41] M. Cascetta, F. Licheri, R.P. Merchán, M. Petrollese, Operating performance of a joule-Brayton pumped thermal energy storage system integrated with a concentrated solar power plant, Journal of Energy Storage 73 (Dec. 2023) 108865, https://doi.org/10.1016/j.est.2023.108865.
[42] H. Jockenhöfer, W.-D. Steinmann, D. Bauer, Detailed numerical investigation of a pumped thermal energy storage with low temperature heat integration, Energy 145 (Feb. 2018) 665–676, https://doi.org/10.1016/j.energy.2017.12.087.
[43] S. Barberis, S. Maccarini, S.S.M. Shamsi, A. Traverso, Untapping industrial flexibility via waste heat-driven pumped thermal energy storage systems, Energies 16 (17) (Jan. 2023), https://doi.org/10.3390/en16176249. Art. no. 17.
[44] D. Alfani, M. Binotti, E. Macchi, P. Silva, M. Astolfi, sCO2 power plants for waste heat recovery: design optimization and part-load operation strategies, Appl. Therm. Eng. 195 (Aug. 2021) 117013, https://doi.org/10.1016/j.applthermaleng.2021.117013.
[45] M. Biondi, A. Giovannelli, G. Di Lorenzo, C. Salvini, Techno-economic analysis of a sCO2 power plant for waste heat recovery in steel industry, Energy Rep. 6 (Dec. 2020) 298–304, https://doi.org/10.1016/j.egyr.2020.11.147.
[46] S. Trevisan, S.S.M. Shamsi, S. Maccarini, S. Barberis, R. Guedez, Techno-economic assessment of CO2-based power to heat to power Systems for Industrial Applications, J. Eng. Gas Turbines Power 145 (121008) (Oct. 2023), https://doi.org/10.1115/1.4063418.
[47] R. Guédez, et al., Design of a 2 MW molten salt driven supercritical CO2 cycle and turbomachinery for the SOLARSCO2OL demonstration project, in: Presented at the ASME Turbo Expo 2022: Turbomachinery Technical Conference and Exposition, American Society of Mechanical Engineers Digital Collection, Oct. 2022, https://doi.org/10.1115/GT2022-82013.
[48] M. Petrollese, M. Cascetta, V. Tola, D. Cocco, G. Cau, Pumped thermal energy storage systems integrated with a concentrating solar power section: conceptual design and performance evaluation, Energy 247 (May 2022) 123516, https://doi.org/10.1016/j.energy.2022.123516.
[49] J. McTigue, P. Farres-Antunez, K. Ellingwood, T. Neises, A. White, Pumped thermal electricity storage with supercritical CO2 cycles and solar heat input, AIP Conf. Proc. 2303 (1) (Dec. 2020) 190024, https://doi.org/10.1063/5.0032337.
[50] G.F. Frate, A. Baccioli, L. Bernardini, L. Ferrari, Assessment of the off-design performance of a solar thermally-integrated pumped-thermal energy storage, Renew. Energy 201 (Dec. 2022) 636–650, https://doi.org/10.1016/j.renene.2022.10.097.

[51] S.S.M. Shamsi, S. Maccarini, S. Trevisan, S. Barberis, R.E. Guedez Mata, "sCO2 Based Pumped Heat Thermal Energy Storage Systems Valorizing Industrial Waste Heat Recovery: A Techno-Economic Analysis of the Role of High Temperature TES," presented at the ASME Turbo Expo 2023: Turbomachinery Technical Conference and Exposition, American Society of Mechanical Engineers Digital Collection Sep, 2023, https://doi.org/10.1115/GT2023-103080.

[52] M. Zhang, et al., Configuration mapping of thermally integrated pumped thermal energy storage system, Energy Convers. Manag. 294 (Oct. 2023) 117561, https://doi.org/10.1016/j.enconman.2023.117561.

[53] S. Hu, Z. Yang, J. Li, Y. Duan, Thermo-economic analysis of the pumped thermal energy storage with thermal integration in different application scenarios, Energy Convers. Manag. 236 (May 2021) 114072, https://doi.org/10.1016/j.enconman.2021.114072.

[54] S. Guccione, S. Trevisan, R. Guedez, B. Laumert, S. Maccarini, A. Traverso, "Techno-Economic Optimization of a Hybrid PV-CSP Plant With Molten Salt Thermal Energy Storage and Supercritical CO2 Brayton Power Cycle," presented at the ASME Turbo Expo 2022: Turbomachinery technical conference and exposition, American Society of Mechanical Engineers Digital Collection Oct, 2022, https://doi.org/10.1115/GT2022-80376.

[55] P. Tafur-Escanta, R. Valencia-Chapi, M. López-Guillem, O. Fierros-Peraza, J. Muñoz-Antón, Electrical energy storage using a supercritical CO2 heat pump, Energy Rep. 8 (Jun. 2022) 502–507, https://doi.org/10.1016/j.egyr.2022.01.073.

[56] Inconel Ball Valves | Alloy 600/ 625 Hydraulic Ball Valve Manufacturer, Accessed: May 21, 2024. [Online]. Available: https://www.oshwin.com/inconel-ball-valves.html.

[57] W. Li, Z. Yu, Heat exchangers for cooling supercritical carbon dioxide and heat transfer enhancement: a review and assessment, Energy Rep. 7 (Nov. 2021) 4085–4105, https://doi.org/10.1016/j.egyr.2021.06.089.

[58] G.O. Musgrove, D. Shiferaw, S. Sullivan, L. Chordia, M. Portnoff, Heat Exchangers for Supercritical CO2 Power Cycle Applications, 2024.

[59] S. Trevisan, R. Guédez, B. Laumert, Thermo-economic optimization of an air driven supercritical CO2 Brayton power cycle for concentrating solar power plant with packed bed thermal energy storage, Sol. Energy 211 (Nov. 2020) 1373–1391, https://doi.org/10.1016/j.solener.2020.10.069.

[60] FRAGOLTHERM® X-75-A - FRAGOL, Accessed: Jan. 05, 2023. [Online]. Available: https://www.fragol.de/en/heat-transfer-fluids/silicone-oils/products/fragoltherm-x-75-a.html.

[61] FME HighEFF. Centre for an Energy Efficient and Competitive Industry for the Future - PDF Free Download, Accessed: Jan. 05, 2023. [Online]. Available: https://docplayer.net/204004398-Fme-higheff-centre-for-an-energy-efficient-and-competitive-industry-for-the-future.html.

[62] A. Caraballo, S. Galán-Casado, Á. Caballero, S. Serena, Molten salts for sensible thermal energy storage: a review and an energy performance analysis, Energies 14 (4) (Jan. 2021), https://doi.org/10.3390/en14041197. Art. no. 4.

[63] Welcome to CoolProp — CoolProp 6.4.3 documentation, Accessed: Jan. 04, 2023. [Online]. Available: http://www.coolprop.org/.

[64] G. Baglietto, S. Maccarini, A. Traverso, P. Bruttini, Techno-economic comparison of supercritical CO2, steam, and organic Rankine cycles for waste heat recovery applications, J. Eng. Gas Turbines Power 145 (4) (Dec. 2022), https://doi.org/10.1115/1.4055727.

[65] A.A. Kebede, T. Kalogiannis, J. Van Mierlo, M. Berecibar, A comprehensive review of stationary energy storage devices for large scale renewable energy sources grid integration, Renew. Sust. Energ. Rev. 159 (May 2022) 112213, https://doi.org/10.1016/j.rser.2022.112213.

[66] E.T. Sayed, et al., Renewable energy and energy storage systems, Energies 16 (3) (Jan. 2023), https://doi.org/10.3390/en16031415. Art. no. 3.

[67] E. Rosenlieb, D. Heimiller, S. Cohen, Closed-Loop Pumped Storage Hydropower Resource Assessment for the United States. Final Report on HydroWIRES Project D1: Improving Hydropower and PSH Representations in Capacity Expansion Models, 2024.

[68] N.T. Weiland, B.W. Lance, S.R. Pidaparti, "sCO2 Power Cycle Component Cost Correlations From DOE Data Spanning Multiple Scales and Applications," presented at the ASME Turbo Expo 2019: Turbomachinery Technical Conference and Exposition, American Society of Mechanical Engineers Digital Collection Nov, 2019, https://doi.org/10.1115/GT2019-90493.

[69] H. Zhao, Q. Deng, W. Huang, D. Wang, Z. Feng, Thermodynamic and economic analysis and multi-objective optimization of supercritical CO2 Brayton cycles, J. Eng. Gas Turbines Power 138 (081602) (Mar. 2016), https://doi.org/10.1115/1.4032666.

[70] C.K. Ho, M. Carlson, P. Garg, P. Kumar, "Cost and performance tradeoffs of alternative solar-driven S-CO2 Brayton cycle configurations," Presented at the ASME 2015 9th International Conference on Energy Sustainability Collocated with the ASME 2015 Power Conference, the ASME 2015 13th International Conference on Fuel Cell Science, Engineering and Technology, and the ASME 2015 Nuclear Forum, American Society of Mechanical Engineers Digital Collection, Oct. 2015, https://doi.org/10.1115/ES2015-49467.